JOURNAL OF GEOPHYSICAL RESEARCH, VOL. 106, NO. B4, PAGES 6325-6345, APRIL 10, 2001

Magnetic anomaly interpretation across the southern central Andes (32°-34°S): The role of the Juan Fernández Ridge in the late Tertiary evolution of the margin

Gonzalo A. Yáñez[1]
Servicio Nacional de Geología y Minería, Santiago, Chile

César R. Ranero, Roland von Huene, and Juan Díaz[2]
GEOMAR, Christian Albrechts Universität, Kiel, Germany

Abstract. Marine and terrestrial magnetic surveys have been integrated to study the tectonic structure of the convergent margin of Chile between 32°-34° S. Three magnetic domains have been identified: oceanic, continental margin, and subaerial. The oceanic domain has seafloor spreading anomalies (16 (~37 Ma) to 18 (~39.5 Ma)) disturbed by anomalies of the Juan Fernandez hot spot chain. In the continental margin, the most prominent fabric are E-W anomalies in the upper slope corresponding to onshore E-W anomalies of large intrusive bodies. Onshore, a N-S lineament of short-wavelength anomalies defines the roots of a Cretaceous volcanic arc. A resembling lineament offshore indicates a submerged older volcanic arc and that continental basement extends to ~50 km landward of the trench. Absolute Cenozoic plate motion for Nazca and South American plates and dating of the Juan Fernandez chain provide a kinematic model of ridge-continent collision. The reconstruction indicates rapid southward migration of the collision point along ~1400 km of the margin from 20 to 11 Ma (~20 cm yr^{-1}). From 11 Ma to present the collison point has migrated at a slower rate along ~ 375 km of the margin (3.5 cm yr^{-1}). The predicted location of the subducted portion of the Juan Fernandez chain coincides with the south edge of the southward migrating flat slab segment of the subducted lithosphere and with a cluster of deep earthquakes indicating a causal relationship. In the last ~10 Myr the ridge has separated a sediment starved trench to the north where subduction erosion may dominate from a sediment filled trench to the south where recent sediment accretion dominates. These observations indicate that subduction of the Juan Fernández chain plays a major role in arc-forearc tectonics.

1. Introduction

The first-order influence of subduction over continental geology and tectonism in the western margin of South America has been established from different lines of reasoning. *Barazangi and Isacks* [1976] described the shape of the subducting slab, correlating changes in the dip angle of subduction with zones where present volcanism was absent (flat slab) or active (deep slab) (Figure 1). *Jordan et al.* [1983] show that these seismotectonic segments also determined the style of foreland tectonism and geomorphology of the active margin. Major features of tectonic segmentation of the Andes are the thin skin versus thick skin foreland thrust fault system in the steep and flat slab segments, respectively. Steep slab segments also include the development of a central depression (Figure 1). At a broader scale, *Pardo-Casas and Molnar* [1987] determined that periods of high convergence between the Nazca and South American plates correlate with periods of relatively high tectonism in the Andes. On the other hand, *Sillitoe* [1974] and *Davidson and Mpodozis* [1991] show the association between subduction and arc-related mineral deposits. They established the link between periods of quiescent magmatism and development of world-class deposits.

The origin of the flat slab geometry is debated and not yet understood. The geographical association between the Nazca and Juan Fernández ridges with the flat slab segments of the Andes (Figure 1) have been used by *Pilger* [1981] and *Nur and Ben-Avraham* [1981], among others, to argue in favor of a causative relationship. According to their model the buoyancy of the corresponding subducted ridges would cause the flat slab geometry. In contrast, *Cahill and Isacks* [1992] consider that the flat slab geometry is related to the curvature of the margin and thus relate control to the continental rather than the oceanic plate.

Tectonic erosion and accretion of the margin have been documented by *von Huene and Scholl* [1991], establishing the role played by each subduction process. The amount of sediments in the trench, the convergence rate, and other factors seem to control the growth or destruction of the margins. Evidence of tectonic erosion back in time has been documented to the north of 33.5°S [e.g., *Rivano et al.*, 1985; *Mpodozis and Ramos*, 1989; *Stern and Mpodozis*, 1991] with a consistent eastward magmatic arc migration since Meso-Cenozoic times. South of 33.5°S the margin appears almost stationary, with a delicate balance between accretion and erosion [e.g., *Mpodozis and Ramos*, 1989]. This major tectonic boundary at 33.5°S also coincides with a Mesozoic boundary in the upper plate (Figure 1). In addition, the Juan Fernández Ridge is now colliding against the margin at the same tectonic boundary (Figure 1).

Above we show how several first-order geological elements converge at this major tectonic boundary during a long range of the Andean cycle. The link between them, if not a simple coincidence, suggests the action of preexisting/inherited

[1]Now at GEODATOS SAIC, Santiago, Chile.
[2]Now at School of Ciencias del Mar, Universidad Católica de Valparaíso, Valparaíso, Chile.

Paper number 2000JB900337.
0148-0227/01/2000JB900337$09.00

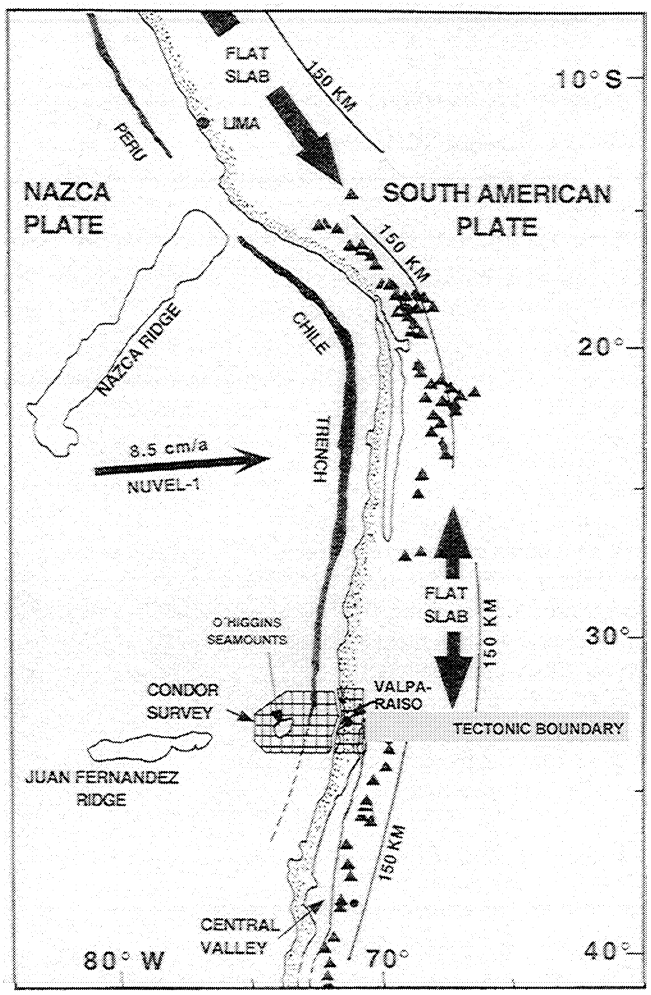

Figure 1. Present Andean tectonic configuration. Solid triangles indicate active volcanism. The 150-km contour lines in the continent show the depth to the Wadati-Benioff plane. The area of this study is highlighted in the region nearby Valparaiso. The Chile Trench south of 33°S is not present due to an almost complete sediment infill.

geological conditions in the continental plate [e.g., *Yáñez*, 1995], and/or a quasi-stable interaction with the Aluk/Nazca plate and the likely presence of passive and active ridges.

The role played by the collision and subduction of an aseismic ridge could be a fundamental one; however, a connection between both phenomena has not been established. To better understand this problem, we have analyzed geophysical data, mostly regional magnetics, onshore and offshore the tectonic boundary (Figure 1), integrated with seismic data, geology, topography/bathymetry, and seismicity. Reliable and consistent magnetic coverage of the margin between 32° and 34°S allows the magnetic characterization of the main tectonic features. Two-dimensional (2-D) and 3-D magnetic modeling of the ocean crust provides a precise age for the oceanic plate and the timing of the volcanism along the Juan Fernández chain (Figure 1). With this information a refined Nazca-South America plate reconstruction for the Miocene is derived. The effects of the Juan Fernández Ridge collision and subduction are analyzed from the perspective of the associated geological effects, the magnetic and seismic response of different geological units across strike, and their correlation with the observed topographic relief. Within this analysis we identify a series of magnetic domains with distinctive geological and tectonic patterns. The magnetic domains are further analyzed and described using a pseudosusceptibility inversion of the magnetic map.

The area of study is located between 32° and 34°S (Figures 1 and 2). The Nazca plate is presently being subducted beneath the South American plate almost at right angles, with a convergence velocity of ~8.5 cm yr^{-1} [e.g., *De Mets et al.*, 1990]. The age of the oceanic crust at the trench varies from Eocene in the north (~32°S) to Oligocene at 34°S (Figure 2), reflecting the oblique tectonic configuration of the margin prior to early Oligocene [*Cande and Leslie*, 1986]. The dip angle of the Wadatti-Benioff plane defines a north segment of "shallow" subduction (~ 10°-15°, the flat segment), and a southern segment of "normal" subduction (~30°) [*Cahill and Isacks*, 1992]. Volcanism is active in the southern segment due to a well-developed asthenospheric wedge. In the flat slab segment, volcanism is absent during the last 10 Myr. From a geochemical perspective, *Kay et al.* [1991] argue that the flat slab configuration started prior to 18 Ma in the north (~28°S) and propagated southward in the following 10 Myr.

The Juan Fernández Chain constitutes a discontinuous array of volcanic centers aligned roughly E-W (Figure 1). The origin of this volcanic aseismic ridge has been attributed to a hot spot located to the east of Alejandro Selkirk Island (see location in Figure 2 [from *von Huene et al.*, 1997]). Free air gravity response of the aseismic ridge (Figure 2) shows a continuous positive anomaly flanked by a broader negative anomaly in each side, as a result of the flexural loading of the oceanic crust. The eastward projection of the aseismic ridge roughly coincides with the miniorocline bending of the continent (Figure 2). The northern edge of the central depression is also coincident with this continental bending and tectonic boundary (Figures 2 and 3). The trench morphology (Figures 3 and 4) evolves from a narrow and almost empty trench north of ~33°S to a relatively wide turbidite-filled trench southward. Other important geographical and geomorphological features cited in the text are shown in Figure 3 with the topography/bathymetry of the study area.

2. Magnetic Data Processing

Two regional magnetic data sets are merged in this study. Offshore magnetic data were acquired during the Condor project with the R/V *Sonne* [*von Huene et al.*, 1997]. The survey collected 12,000 linear km along E-W tracks, with a line spacing of 3 km in shallow bathymetry and 6 km over the deep ocean. On the continent, the Chilean Geological Survey (Sernageomin) acquired lines flown N-S at a constant clearance of ~1 km and a nominal line spacing of 2.5-3 km. The information accuracy in both data sets is similar. We estimate an error envelope of 10 nT (see *Yáñez et al.* [1995] and *Parra and Yáñez* [1988] for thorough reviews of technical specifications in oceanic and continental surveys, respectively). Only a corridor of 12 miles (20 km) off the shoreline remains without magnetic information to date. Minor line effects in regions of low magnetic amplitude were further filtered using decorrugation filters and robust microleveling [*Yáñez et al.*, 1995]. The Condor project also provided a high-resolution bathymetry of the region (~10 m) that can be linked with digital terrain models of the subaerial region, extracted from 1:50,000 topographic charts (see contour lines in Figure 3).

The main distortion in the magnetic data is due to the variable distance from the observation point to the magnetic source (the crustal surface in general). As we can observe in Figure 3, this distance ranges from more than 6000 m at the trench to 500 m near the O'Higgins seamount, with extensive areas of oceanic crust at an average depth of 4500 m. On the other hand, continental regions were flown much closer to the causative bodies, keeping a roughly constant clearance of 1000 m. Thus the first step in magnetic data processing involved the continuation of the data to a common distance above the crustal surface. In order to accomplish the continuation to an arbitrary surface we implemented the 2-D algorithm of *Hansen and Miyazaki* [1984]. A 2-D continuation algorithm is certainly an appropriate tool for

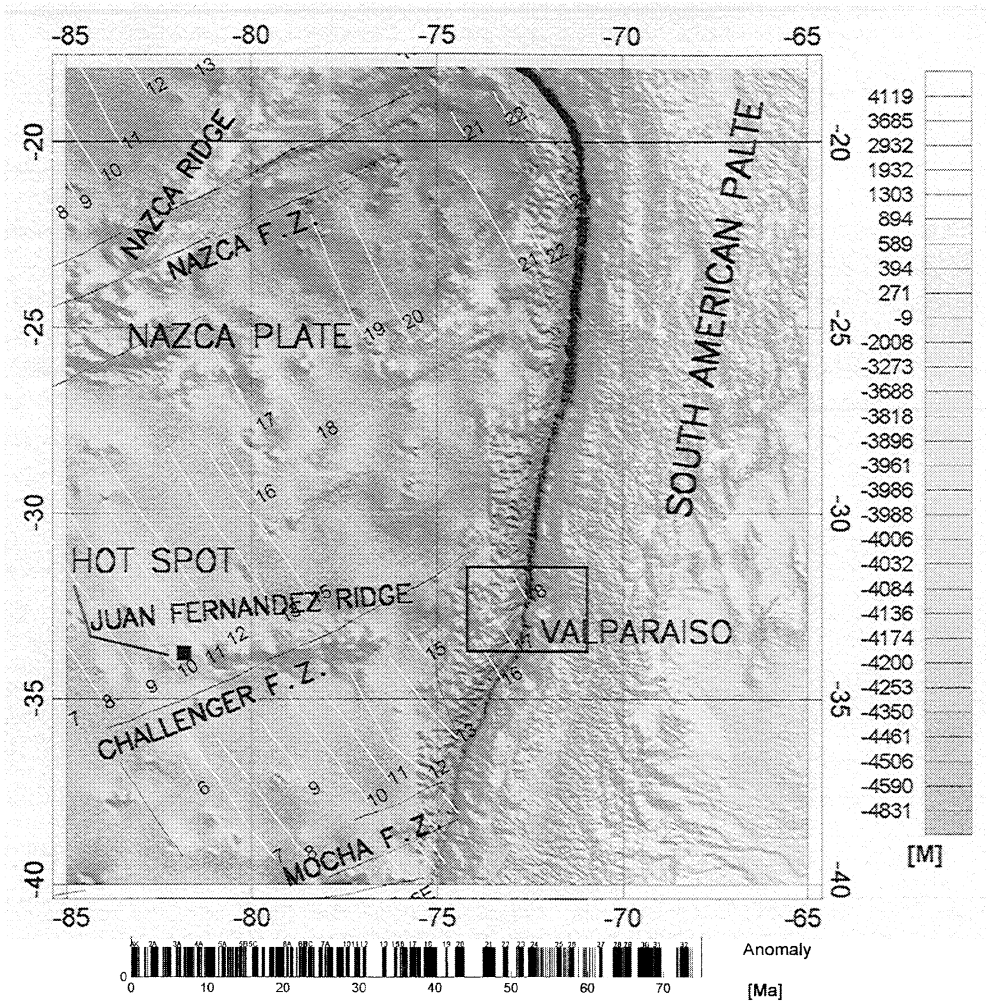

Figure 2. Regional framework of the Nazca-South America plate interaction over a digital terrain model of the continental and oceanic plates. The heavy line box indicates the area of the present study, and the location of the Juan Fernández hot spot from *von Huene et al.* [1997]. Major features in the continental area are the Altiplano Orocline and the high Altiplano Plateau the width and altitude of which decrease southward. To the south of the study area a miniorocline indicates the segmentation boundary at 33.5°S and also the begining of the central valley. In the ocean plate, the Juan Fernández Ridge shows the typical flexural pattern associated with the load of a volcanic chain (a relative high flanked by a pair of longer-wavelength lows). When the chain approaches the margin the pattern vanishes due to the downward bending of the Nazca plate and the flexure due to the change in orientation of the trench. White lines represent the seafloor magnetic anomalies, with their corresponding numbers.

most of the oceanic region under analysis except for the seamount chain. However these volcanic edifices are almost at the same distance from the desired continuation level, and therefore the errors will be minor. In this method we have to find the equivalent magnetic layer intensity ($\mu(\xi_i)$) by solving the discretized matrix system:

$$\phi(x_j) = \frac{1}{\pi} \sum_{i=j-\Delta}^{j+\Delta} \mu(\xi_i) \int_{\xi_i-\delta/2}^{\xi_i+\delta/2} \frac{\hat{v}(\xi_i)\cdot\hat{\rho}}{\rho^2} \frac{d\xi}{n_\varsigma(\xi_i)} \qquad (1)$$

where

$\phi(x_j)$ magnetic total field at xj;

$\hat{v}(\xi_i)$ direction of equivalent ith dipole at position ξ_i;

$n_\varsigma(\xi_i)$ unitary vector normal to the dipole surface at position ξ;

ρ distance from the observation point xj to the ith dipole in the equivalent layer;

$\hat{\rho}$ unitary vector along the direction of ρ;

$\delta/2$ half length of the equivalent magnetic dipole

Δ number of relevant dipoles for the approximation of the magnetic total field at x_j.

The system of equations defined in (1) is solved through singular value decomposition techniques (SVD) [e.g., *Noble and Daniel*, 1977] because downward continuation introduces some numerical instabilities in the matrix inversion. Such a procedure is implemented considering the solution determined only by the largest eigenvalues (10 to 20%). Figure 5 presents an example of the continuation procedure in three profiles (locations of the profiles are indicated in Figure 6b). The example shows how the magnetic signal is amplified where the distance to the source is larger (for instance at the trench). We performed a continuation of the oceanic data 1000 m above the seafloor to have a common clearance distance off shore and onshore. Figure 6b show the processed total field considering leveling and continuation to an

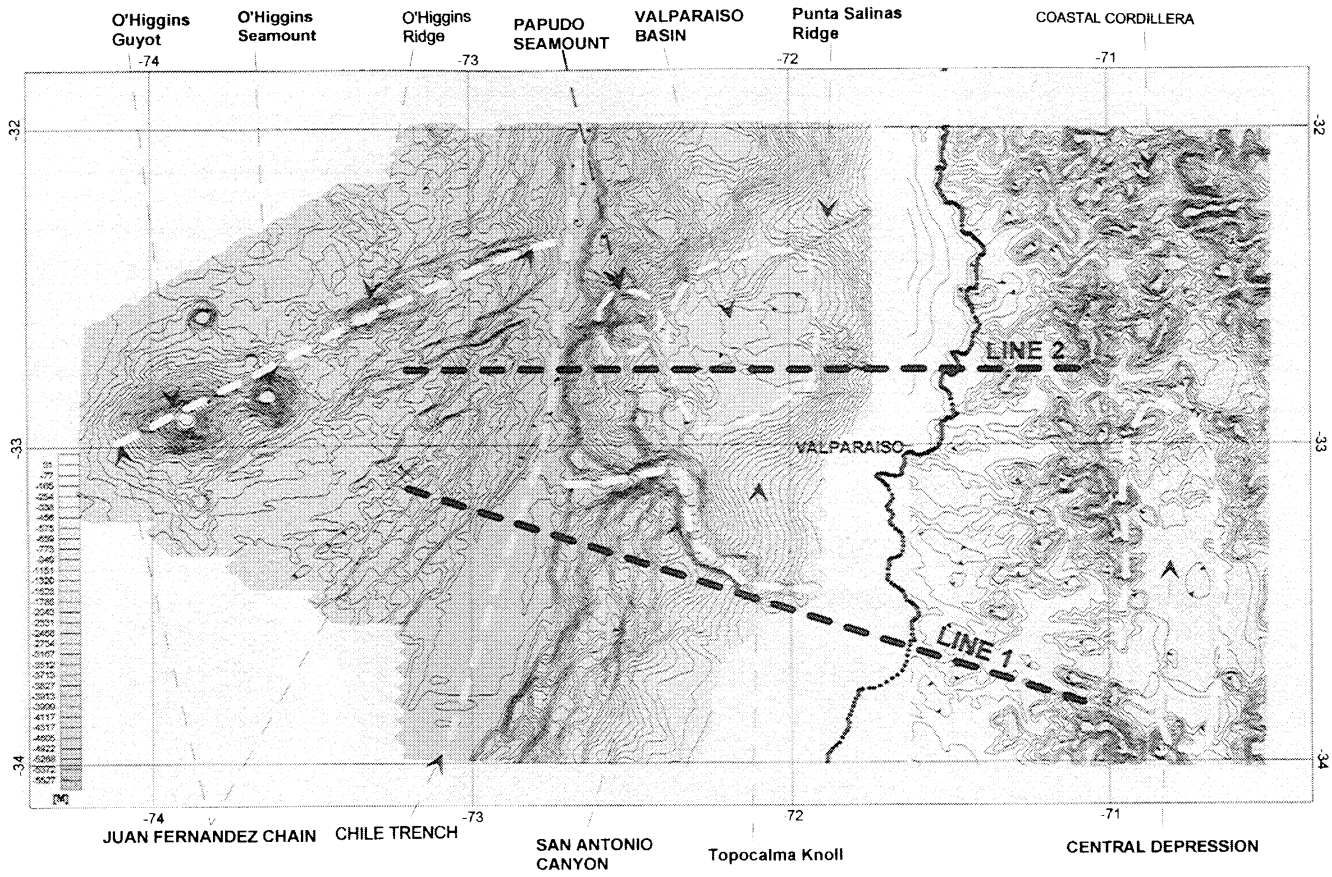

Figure 3. Topography/bathymetry and main locations of the study area. Bathymetry was obtained during Condor cruise [*von Huene et al.*, 1997]. Topography was digitized from 1:50,000 topographic maps. Dashed solid lines (line 1 and line 2) are the location of the wide-angle seismic reflection profiles shown in Figure 10.

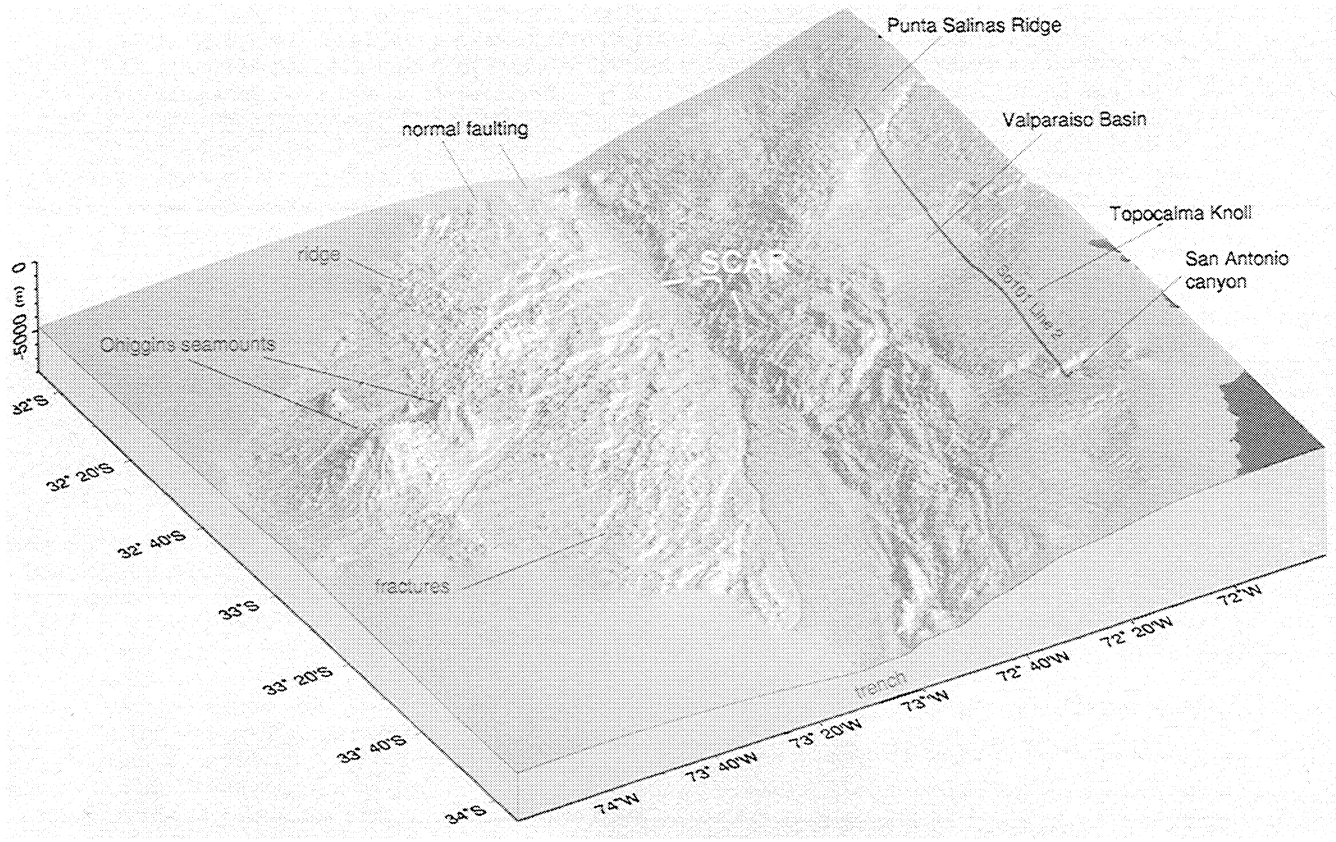

Figure 4. The 3-D high-resolution bathymetry derived from the Condor Project.

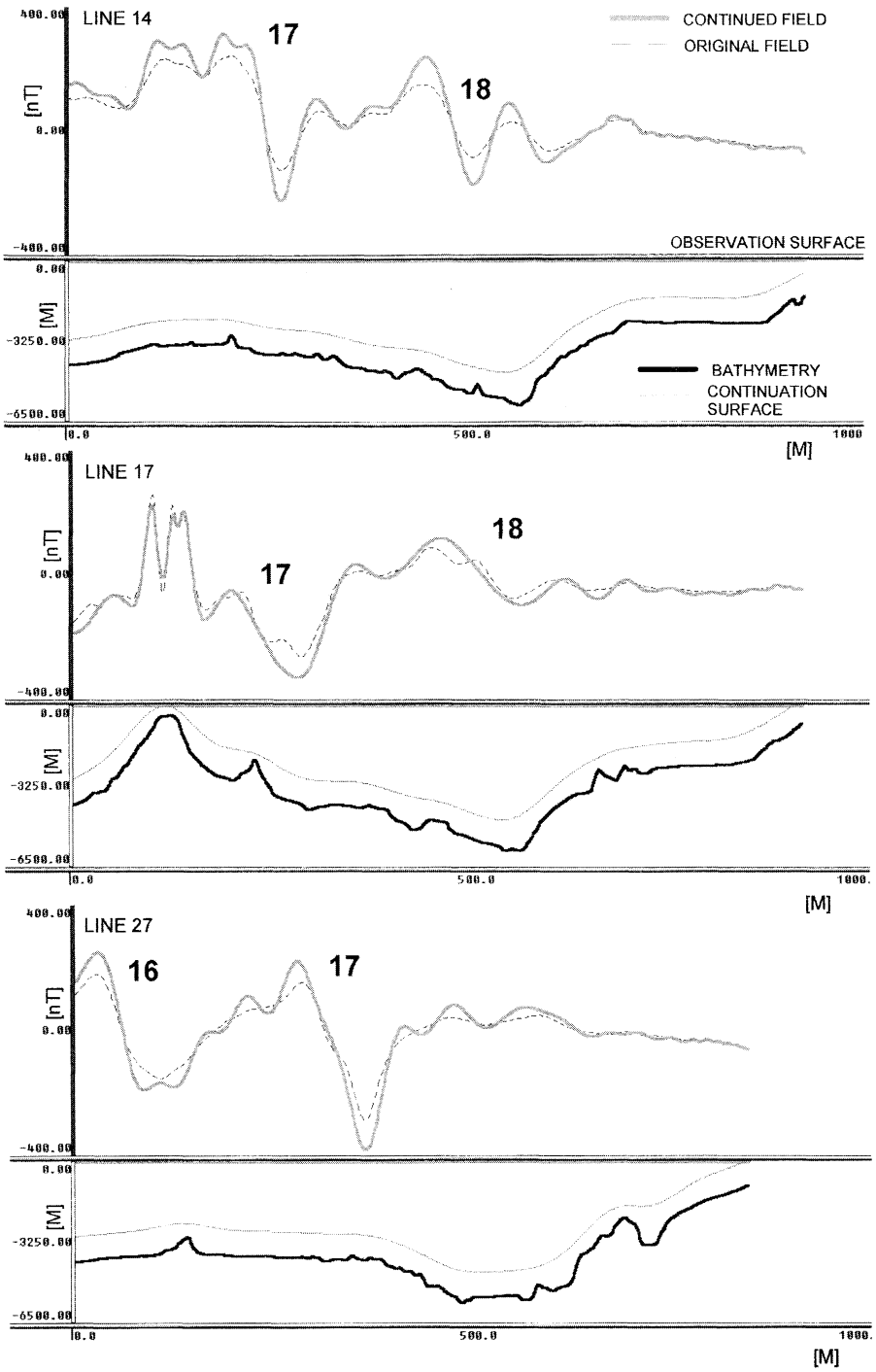

Figure 5. Examples of equivalent source continuation 1000 m above the seafloor in lines 14, 17, 27 (see locations of the lines in Figure 6). In the top panel for each line we show the observed magnetic field (dashed line) and the continuation field (solid line). In the bottom panel we present the corresponding bathymetry (solid line) and the depth of continuation (light line). Numbers in each profile refer to the magnetic anomalies.

arbitrary surface of 1000 m above the seafloor relief. In Figure 6a the original raw data are presented to highlight the improvements of the final product. The composite map of the continental and marine magnetic data sets is presented in Figure 7.

3. Magnetic Modeling

Forward models of major magnetic anomalies were generated to define the geometry, age, depth, and magnetic properties of sources, providing a quantitative tool for the definition of magnetic domains, corresponding to tectonic units (see section 4.1). First, we performed a pseudosusceptibility inversion to establish similarities and differences in the magnetic sources of each data set. In this paper we focus on the poorly known oceanic crust; further modeling of the onshore continental crust can be found elsewhere [e.g., *Parra and Yáñez*, 1988; *Yáñez et al.*, 1998]. A 2-D modeling of the seafloor spreading sequence not perturbed by the Juan Fernández chain volcanism provided dating

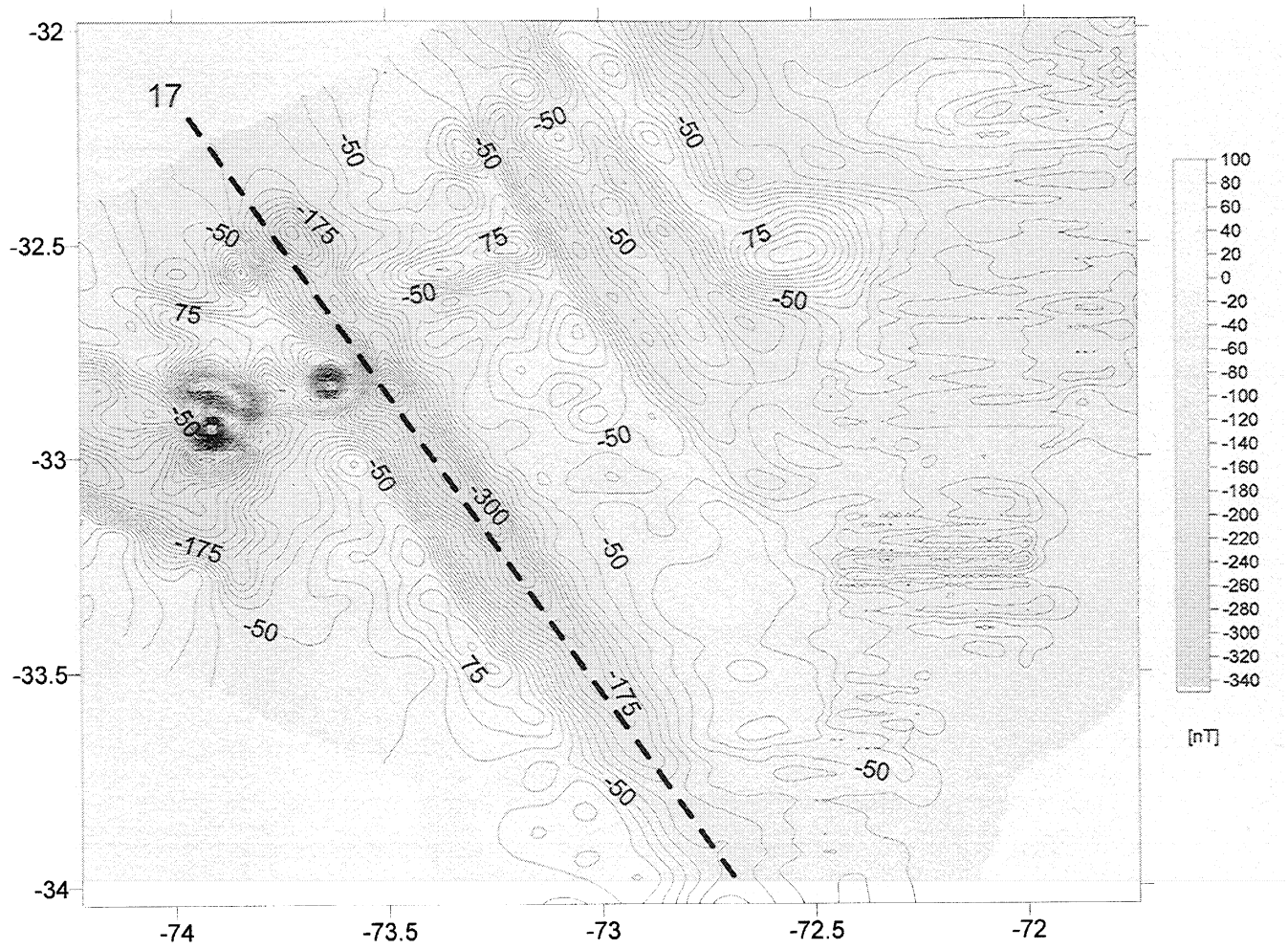

Figure 6a. Raw total magnetic field offshore from Condor cruise.

for the entire section of the Nazca plate under analysis. Subsequently, we incorporated the perturbation of the Juan Fernández volcanoes, considering the available dating for the O'Higgins guyot (8.5 ± 0.4 Ma [*von Huene et al.*, 1997]), and the absolute poles of rotations for the Nazca plate [e.g., *Gordon and Jurdy*, 1986]. In addition, the bending of the ocean plate was also incorporated according to the geometry established by *Flueh et al.* [1998] (see wide-angle seismic reflection results in Figure 10). With all these constraints a full 3-D modeling of the Nazca plate was performed.

3.1. Pseudosusceptibility Inversion

In Figure 8 we present the pseudosusceptibility inversion of the magnetic data produced with the Geosoft™ package. The inversion is achieved considering an array of square prismatic blocks centered at each node of the magnetic grid, with the roof at the surface and infinite in depth. For each block we assumed an induced magnetization vector with inclination and declination of –32° and 4°, respectively, and total magnetic field of 25,000 nT. These parameters are the mean values of the IGRF (International Geomagnetic Reference Field) model for the date and place of the survey area. Although acknowledging that this model is not realistic for the oceanic area, it provides a cross check for the entire survey. In the oceanic plate the magnetic source is mostly restricted to a highly magnetized thin extrusive layer (~500-1000 m), in which thermoremance controls the polarity of the magnetic vectors. We do not consider a chemical remanence as suggested by *Yáñez and Labrecque* [1997], owing to the likely small contribution of intermediate-wavelength anomalies in this rather small magnetic survey. Thus the induced magnetization assumption in the pseudosusceptibility inversion procedure interpreted blocks magnetized during periods of inverse polarity as negative magnetic sources. However, the absolute value of the magnetic susceptibility is basically equivalent to the inversion results in blocks magnetized during periods of normal polarity. The main difference between the oceanic and continental pseudosusceptibility outcome dealt with the well-sorted shape of the oceanic sources, in contrast with the more spotty distribution of the continental flank. This difference is the result of the seafloor spreading process regularity and the more random distribution of magnetic sources in the continent (mostly intrusives according to the geological description of Figure 13). In absolute terms, the pseudosusceptibility is higher in the oceanic crust compare to the continental side (0.04-0.08 SI compared to 0.02-0.04 SI); in addition, we know that oceanic sources are much more restricted in thickness compared to continental sources. These two families of pseudosusceptibility are in good agreement with the mafic source of oceanic crust and the calc-alkaline nature of the continental crust. To first order, the pseudosusceptibility values obtained in the continent are in good agreement with the observed average susceptibilities in outcrops [*Parra and Yáñez*, 1988; *Gana et al.*, 1994]. In this case the causative bodies can be properly treated as "infinite" magnetic sources of 5-10 km thickness. In the oceanic flank the thickness of the magnetic source is probably more than 10 times smaller

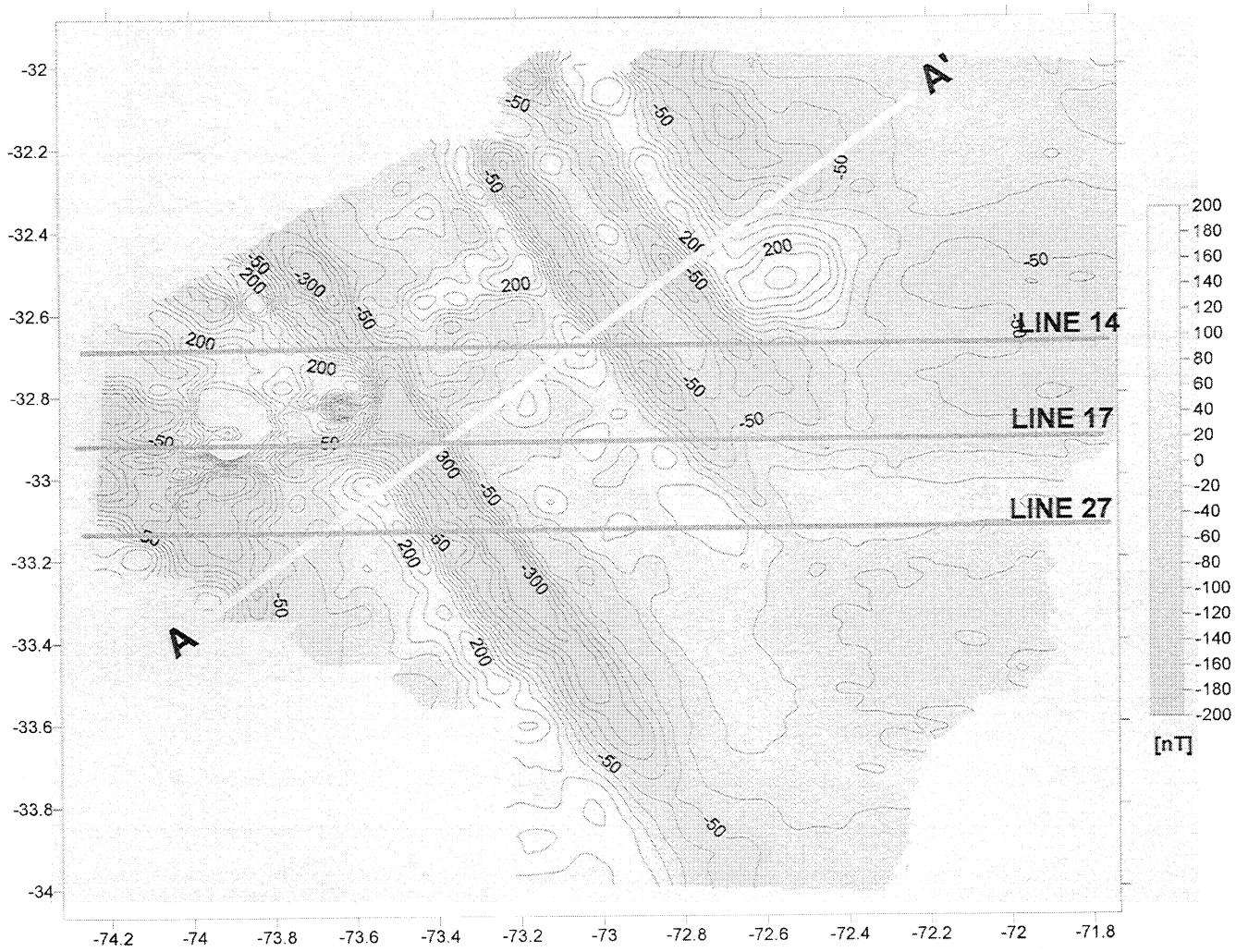

Figure 6b. Corrected total magnetic field offshore, continued 1000 m above the seafloor. Notice the improvement with respect to the raw data set of Figure 6a. The heavy solid lines correspond to the locations of the profiles in Figure 5. The white A-A' line indicates the location of the 2-D magnetic modeling profile.

(except in the seamounts of the Juan Fernández chain), which implies a corresponding increment in the bulk magnetization (discussed in section 3.3).

Major magnetic sources in the continental side are roughly aligned N-S, with a spotty distribution in discrete sources of igneous origin (described in section 4.1.3). The wavelength of the magnetic sources covers a range of 10-30 km. Important E-W magnetic lineations offset the dominant N-S trend implying a postemplacement tectonism.

On the oceanic side, larger magnetic sources trending NW are dramatically reduced in amplitude (more than 1 order of magnitude) east of the trench axis. In the 3-D magnetic model of the oceanic plate (see sections 3.2 and 3.3), we demonstrate that the rapid increment in the distance to the magnetic sources is responsible for this very attenuated magnetic response.

3.2. Seafloor Spreading Anomalies

In this region of the Nazca plate, seafloor spreading magnetic anomalies belong to the Eocene sequence [*Cande and Haxby*, 1991] (see also in Figure 2). The NW direction of this magnetic sequence indicates a highly oblique convergence during the Eocene. The magnetic anomalies identified by *Cande et al.* [1989] range from anomaly 16 to 18 (~36-38 Ma) (Figure 2). We modeled the magnetic sequence along the A-A' profile (see location in Figure 6b), orthogonal with respect to the main magnetic trend and away from magnetic distortions associated with the Juan Fernadez chain. According to *Cande and Haxby* [1991], the half spreading rate of the Nazca plate between anomalies 16 and 18 was ~63 mm yr^{-1}, in good agreement with the Nazca plate velocity in a hot spot reference frame [*Gordon and Jurdy*, 1986]. From the paleoreconstruction of this Nazca plate segment [*Gordon and Jurdy*, 1986], we derived a paleolatitude of –46° at the time of cooling at the spreading center. The common axial magnetic dipole assumption is also considered to set up a paleodeclination of 0°. We considered a volcanic layer of 0.5 km thickness as a single magnetic source, neglecting the effect of gabbros. We adopted a magnetization of 1.5 A m^{-1} in agreement with the observed decay in magnetization for oceanic crust older than 10 Ma [e.g. *Harrison*, 1987]. We used a 2.5-D algorithm implemented in the Model Vision™ package, based on the Talwani's algorithm [e.g., *Telford et al.*, 1990], but constrained along strike (we took a 20-km lateral extension). The resulting forward model is shown in Figure 9. In order to fit the anomalies we had to slightly reduce the half spreading rate determined by *Cande and Haxby* [1991] from 63 to 60 $mmyr^{-1}$. Most of the profile is well resolved in the model, and major discrepancies are observed in the left-hand side (between cumulative distance 16000 and 18000 m in Figure 9). In fact, this sector corresponds to the edge of the survey area and

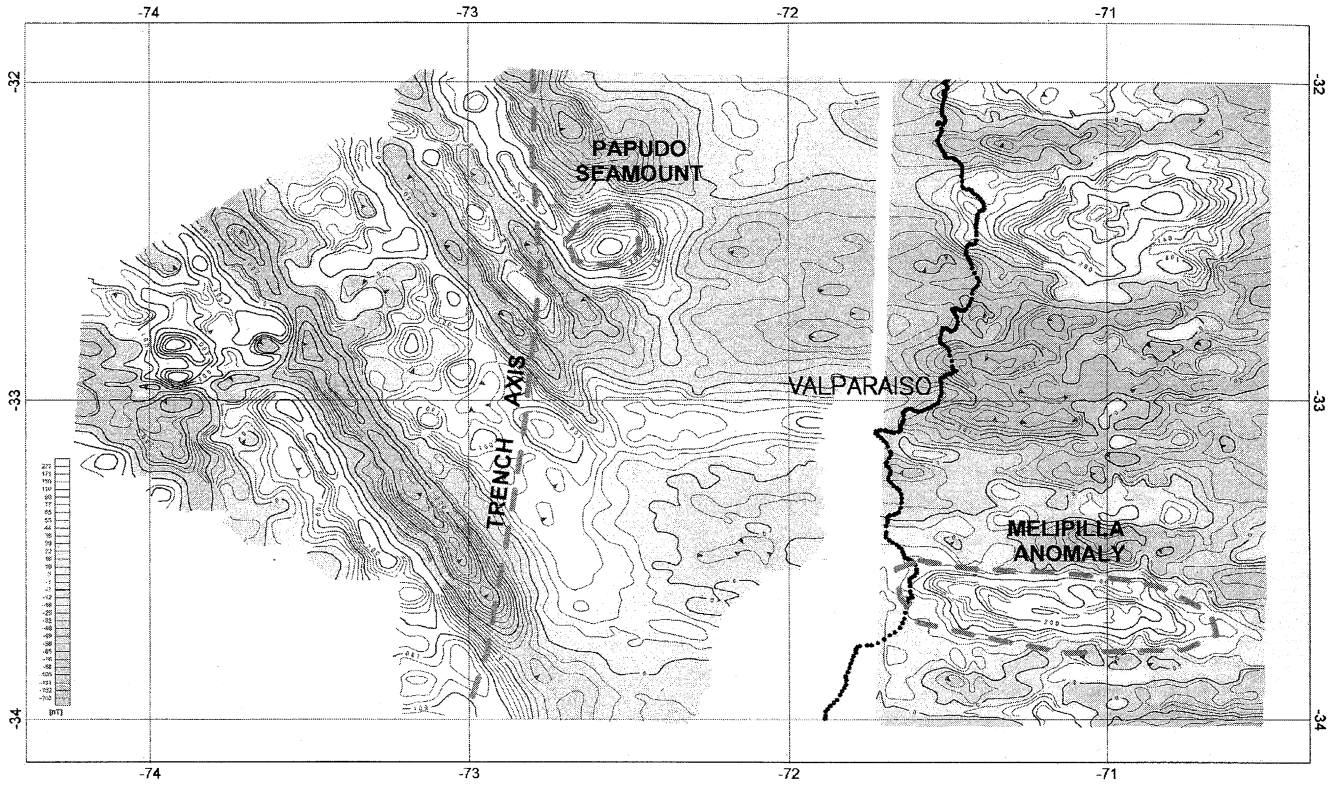

Figure 7. Integrated magnetic field onshore (Sernageomin data set) and offshore (Condor project data set) at 1000 m common level of observation above the relief.

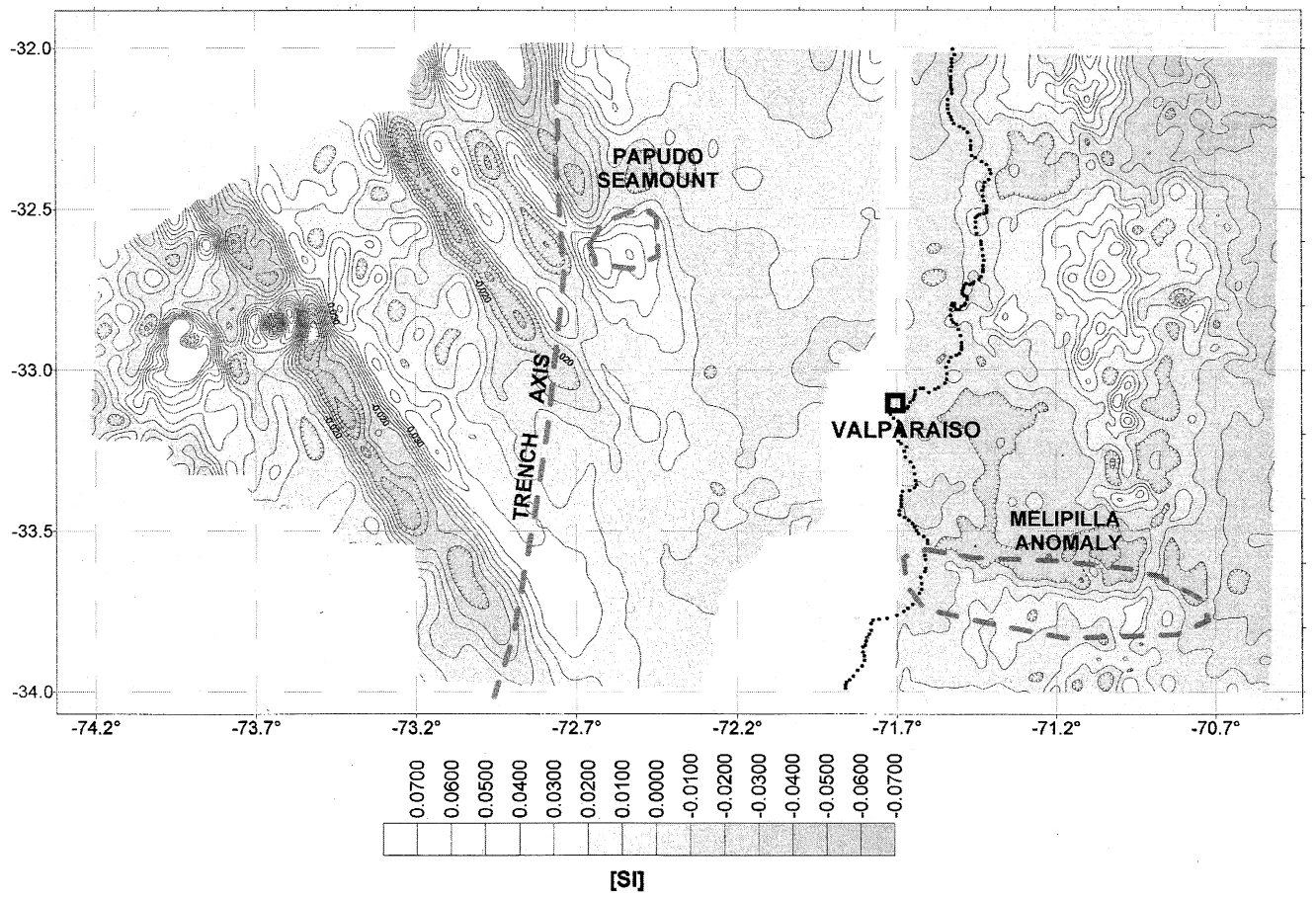

Figure 8. Pseudosusceptibility map derived from composed map of Figure 7.

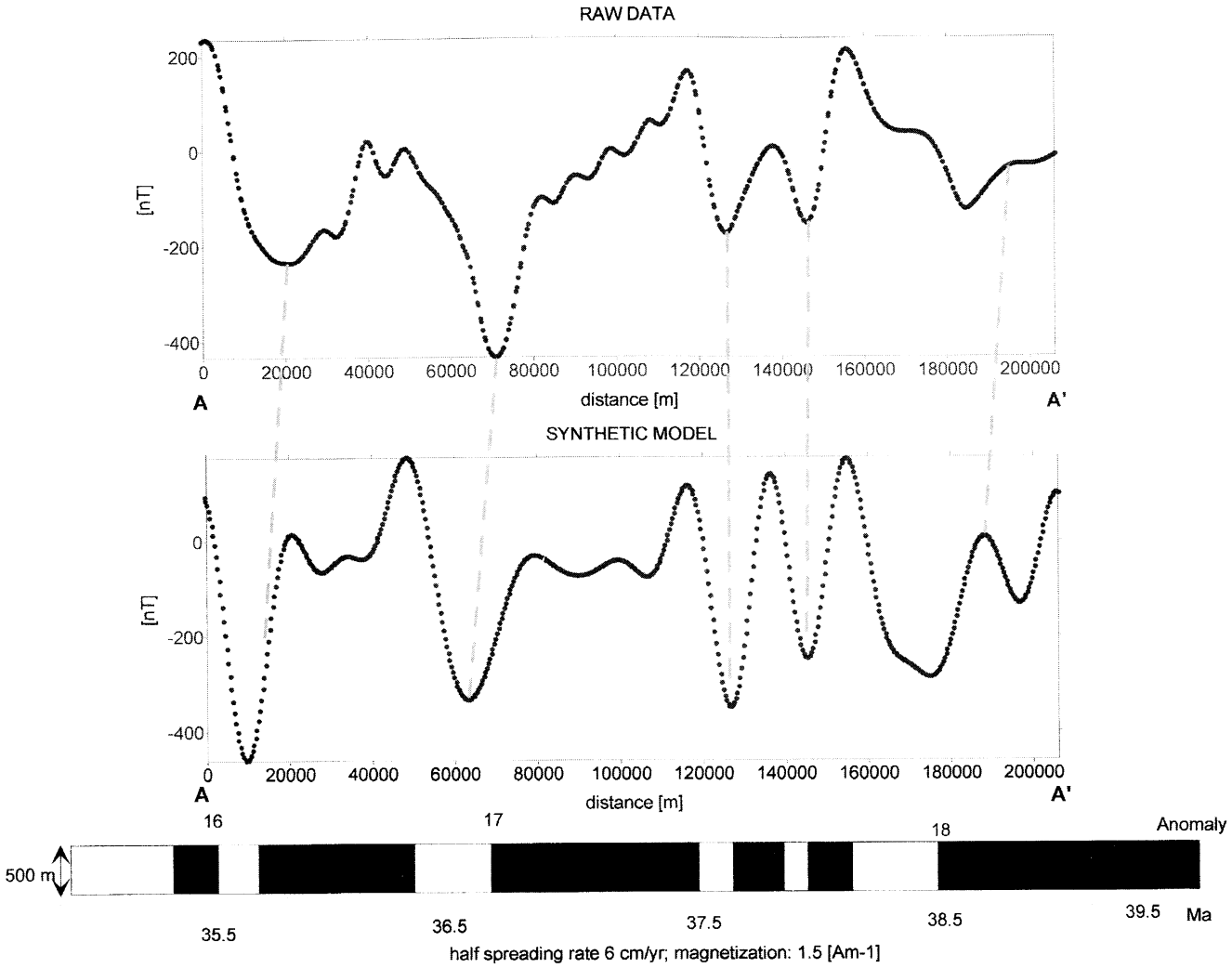

Figure 9. A 2-D magnetic modeling along A-A' profile (see location in Figure 6b). (top) Observed data and (bottom) model result. Segmented lines join equivalent anomalies. At the bottom we show the magnetic polarity timescale (black/white: normal/reverse). The model considers a layer of 500 m magnetized by 1.5 A m^{-1}, with 6 $mmyr^{-1}$ half spreading rate.

also to a region with some perturbation from the O'Higgins seamount signal (see in Figure 6b), and therefore we can expect inconsistencies. However, in the remaining section most of the anomalies are well resolved, despite the simplicity of the model, in which the seafloor relief has not been considered. From this analysis we conclude that the age of the Nazca plate in the region lies in the range of 35.5-39 Ma. This model section is used as a calibration tool for dating of the entire Nazca plate produced by seafloor spreading mechanisms in the study area.

3.3. Three Dimensional Magnetic Modeling

The objective of the 3-D modeling effort was twofold: to determine the magnetic pattern and age of the Juan Fernández chain and the contribution of the subducting slab in the magnetic signal to the east of the trench (Figure 6b). The simplest explanation for the rapid attenuation in the magnetic response of the subducting slab deals with the larger distance to the source. However, other explanations might involve the Curie isotherm; although less likely, the advection of cool isotherms with the slab could be counterbalanced by frictional effects [e.g. *Molnar and England*, 1990]. The dip of the subducting slab beneath the continent was obtained from two wide-angle seismic profiles [*Flueh et al.*, 1998] (see Figure 10). A full 3-D modeling is necessary because the Juan Fernández igneous bodies intruded magnetized oceanic crust of Eocene age. We used the age derived from the 2-D model (Figure 9) to calibrate the age of the oceanic plate by extrapolation along the strike direction and beneath the upper plate (Figure 11a). For the timing of the Juan Fernández chain we have two independent constraints; the "total fusion" age from the O'Higgins guyot of 8.5 ± 0.5 Ma [*von Huene et al.*, 1997] and the Nazca plate reconstruction in a hot spot reference frame [e.g., *Gordon and Jurdy*, 1986, *Pardo-Casas and Molnar*, 1987]. With both sets of independent information we were able to calibrate the age of the Miocene igneous bodies of the Juan Fernández chain. The obtained dating and shape of the oceanic crust under analysis is presented in Figure 11a, and the corresponding magnetic time polarity is shown in Figure 11b.

For the 3-D modeling, we used the magnetization intensity adopted in the previous 2-D modeling: 1.5 A m^{-1} in a magnetized crust of 500 m. The oceanic crust is discretized in prismatic bodies of 2x2 km and horizontal surface on top and bottom. The upper surface of each block is determined by the digital bathymetry of the Nazca plate presented in Figure 10. The magnetic response of each block is determined using the algorithm of *Pluoff* [1975]. Over the Juan Fernández chain we considered blocks 6 times thicker as an approximation of a much thicker volcanic edifice (a more precise modeling effort does not

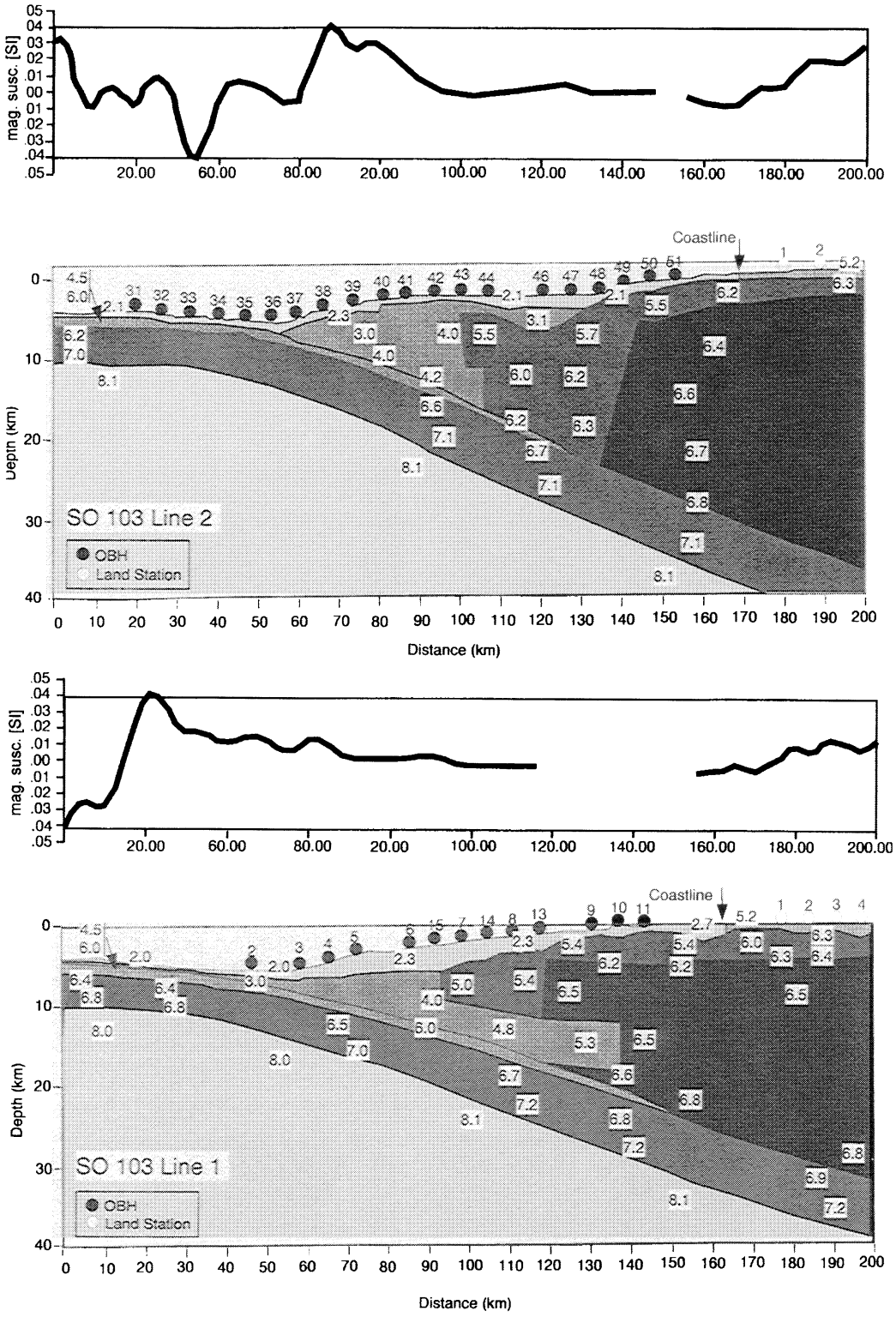

Figure 10. Wide-angle seismic reflections velocity models from *Flueh et al.* [1998]. Locations of the profiles are shown in Figure 3. In the top panel of each profile we include the interpolated pseudosusceptibility profile extracted from Figure 8. The location of the seaward edge of high-velocity bodies (>6.5 km/s) in the upper plate is coincident with a magmatic lineament of magnetic dipoles.

alter the desired first order magnetic response). On the basis of the evidence presented by *von Huene et al.* [1997], together with the Nazca ridge age progression [*O'Connor et al.*, 1995], we assume that the Juan Fernández chain was derived from a hot spot. Precise location of the hot spot is unknown; however, *von Huene et al.* [1997] provide some new evidence for a location to the west of Alejandro Selkirk Island (see location in Figure 2). Magmatic material extruded from the hot spot acquires a thermal remanence in the same way as normal seafloor spreading anomalies. Paleolatitudes for the time of cooling are determined

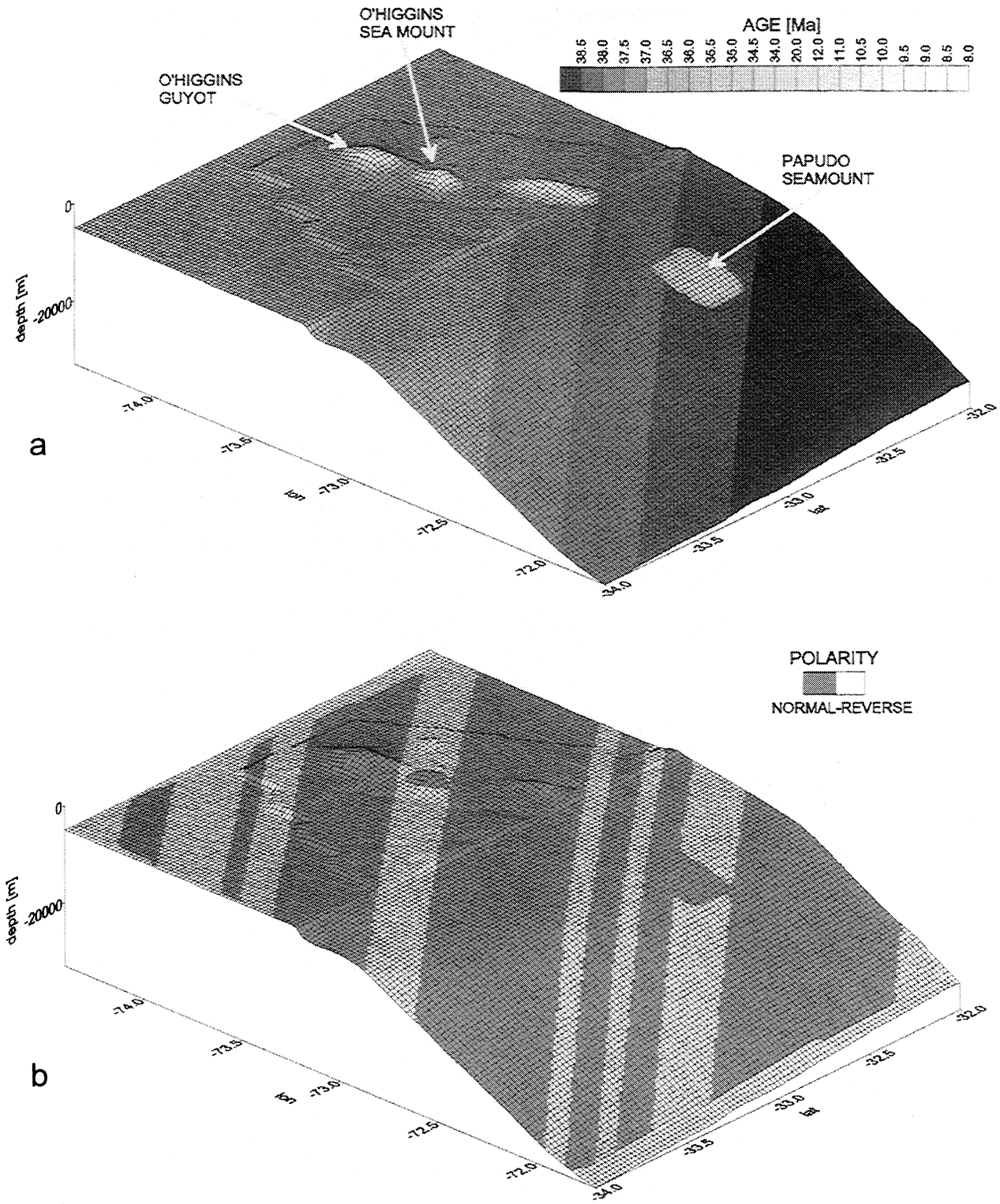

Figure 11. (a) A 3-D view of the shape and age of the Nazca plate and subducting slab. Notice the much younger age of the O'Higgins seamount chain. The shape of the Papudo seamount is the best model result. (b) A 3-D view of the polarity timescale of the model described in Figure 11a. Time polarity scale is from *Cande and Kent* [1994].

by the plate reconstruction in the case of normal oceanic crust, and the location of the hot spot (fixed by definition) for the Juan Fernández chain. The customary axial dipole assumption is considered in both cases (implying a paleodeclination of 0°). For the O'Higgins seamount and guyot (Figure 3), the shape and position of the body are constrained by the bathymetry. The same procedure is considered for the elongated anomaly that follows the Juan Fernández chain to the east. The prominent anomaly located underneath the accretionary prism, the Papudo "subducted" seamount [*von Huene et al.*, 1997], was modeled

with different locations and ages (implying polarity changes). The preferred location and size of the Papudo subducted seamount (in terms of the best adjustment of observations) is presented in Figures 11a and 11b. The final response of the 3-D magnetic model is presented in Figure 12.

Comparing the model response (Figure 12) and the observations (Figures 6a and 6b), we conclude that the main magnetic features are well described by the model. In the normal oceanic crust, the NW trend of the Eocene magnetic sequence decays severely east of the trench, confirming the primary effect of the distance to the magnetic source. In the Juan Fernández chain modeling, we modified the age of the O'Higgins guyot to ~8.7 Ma in order to fit the anomaly with a normal polarity reversal of the magnetic field (Figure 13). Such a small change in age with respect to the analytical estimate of 8.5 Ma fits inside the error envelope of 0.4 Ma [*von Huene et al.*, 1997]. The O'Higgins seamount is also modeled within the period of normal polarity in anomaly 4A (8.66-9 Ma), although it seems that the central part might be cooled later during a period of reverse polarity (see in Figure 8 the pseudosusceptibility pattern of this area). For the Papudo subducted seamount the plate reconstruction of the Juan Fernández Ridge implies an age of 10.5-10.8 Ma, within a period of normal polarity in the ambient field (see in Figure 2). This timing is in good agreement with the requirement of normal polarity to match the prominent positive magnetic anomaly observed over the Papudo subducted seamount. The size of the causative body is equivalent, if not larger, than the O'Higgins seamount and guyot. The remaining elongated anomaly along the O'Higgins ridge (Figure 3), was also magnetized during a period of normal polarity at the time of cooling. Such a consistency in the polarity of the magnetic field during these episodic magmatic events suggests a causative relationship. The E-W magnetic pattern observed in the accretionary wedge (Figure 7) is not reproduced in the magnetic modeling of the Nazca plate, implying a shallower source within the continental plate.

4. Discussion

4.1. Interpretation of Magnetic Anomalies

We interpret the combined oceanic and continental magnetic data with a focus on the plate interaction. The regional geology has been extracted from *Gana et al.* [1996] and *Rivano et al.* [1990], and the seismic reflection and refraction data are obtained during the Condor project (Figures 10, 13, and 14) are also incorporated in this analysis. In addition, we consider the pseudosusceptibility map described in Figure 8.

The survey area has three different magnetic domains, each with a characteristic magnetic fabric as shown by shape, wavelength, and intensity of magnetic anomalies. Each domain displays predominant magnetic trends or lineations, magnetic

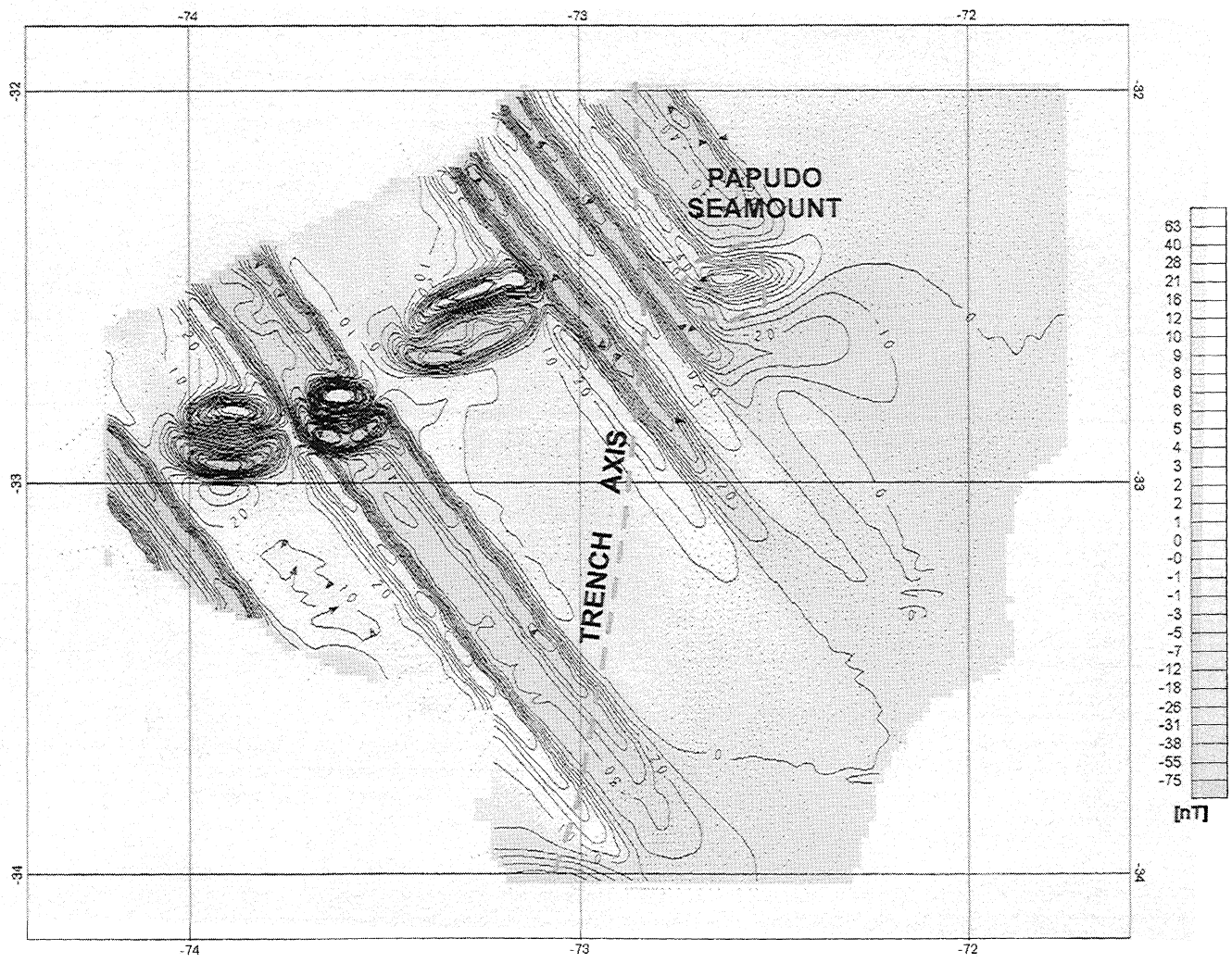

Figure 12. The 3-D magnetic response from model of Figure 11.

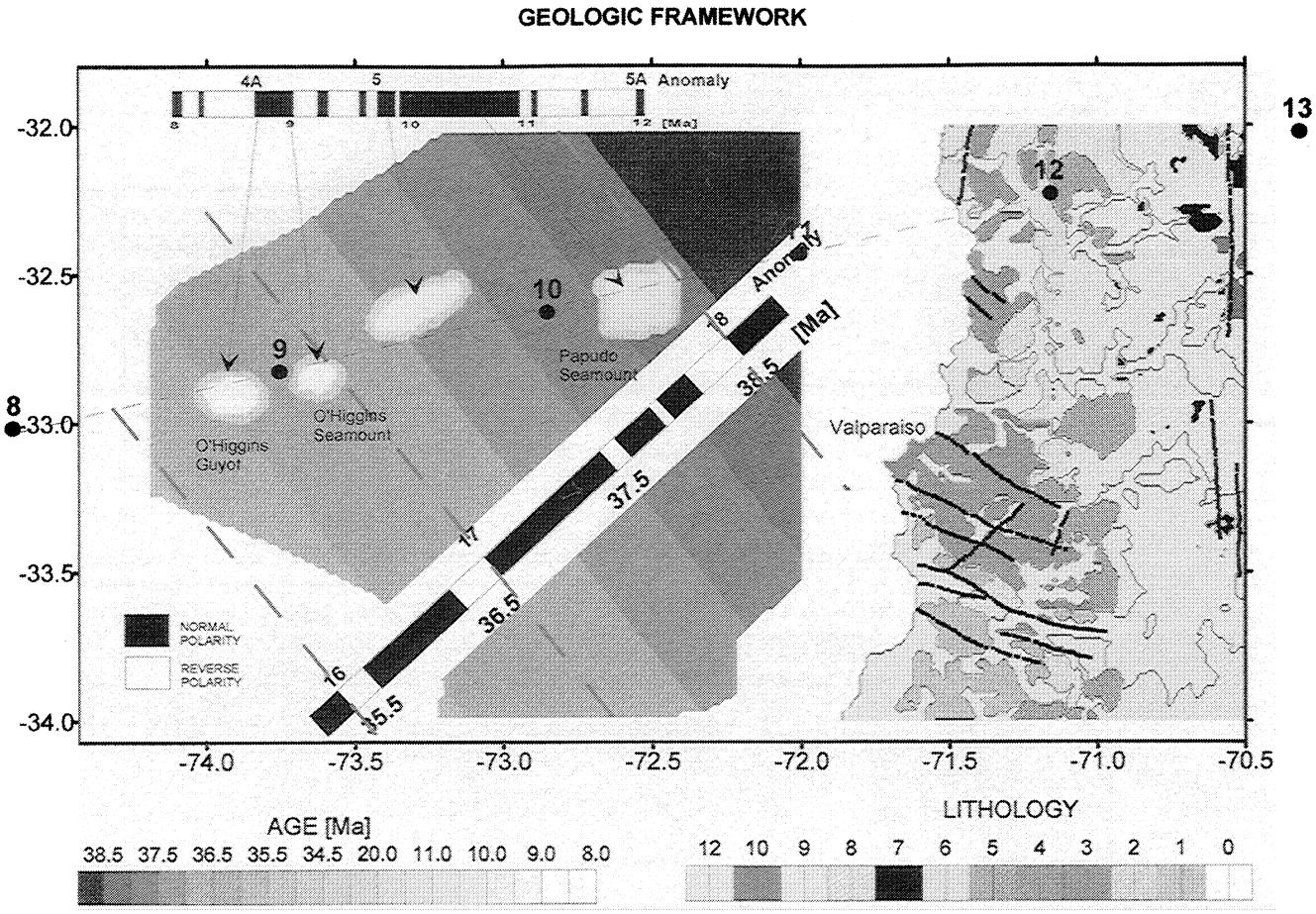

Figure 13. Geological, structural, and geophysical compilation of the study area. In the ocean, information is based on the magnetic data. In the continent, the regional geology have been compiled from *Gana et al.* [1984], *Rivano et al.* [1985], and *Rivano et al.* [1990]. Main geological units are (1) Permo-Carboniferous granitoids; (2) Paleozoic-Jurassic orthogneisses and paragneisses; (3) Jurassic anfibolites and gneisses; (4) Jurassic granitoids; (5) Lower Cretaceous granitoids; (6) Upper Cretaceous-Miocene granitoids; (7) Triassic sedimentary deposits; (8) Jurassic volcanic sequence; (9) Neocomian volcano-sedimentary deposits; (10) Miocene volcanism; (11) Upper Tertiary sedimentary deposits; (12) Quaternary; magnetic lineations (dashed shaded lines); faults and structural lineations (solid lines).

sources, and depth to basement. These domains each have a geological and tectonic character that is characteristic to this segment of the Andean margin.

4.1.1. Oceanic crust domain. The oceanic crust domain is characterized by northwest striking seafloor spreading anomalies. This regular magnetic pattern is superimposed by the episodic volcanism of the Juan Fernández hot spot ridge with a northeast trend.

Considering *Cande and Kent* [1995] timescale, the magnetic modeling of the normal seafloor spreading anomalies (Figure 9) provides a time sequence between anomalies 16 (35.5 Ma) and 18 (38.5-39 Ma) with a half spreading rate of 6 mmyr^{-1}. This rate is in good agreement with the interpretation of *Cande and Haxby* [1991] (6.3 mmyr^{-1}) and consistent with the absolute Nazca plate velocity of *Gordon and Jurdy* [1986] (6.1 mmyr^{-1}).

On the other hand, the superimposed magnetic anomalies associated with the Juan Fernández seamount chain are largely, if not completely, explained by the volcano edifices of the area (Figure 13). This major volcanic trend is cut at nearly right angles by subtle trend of smaller seamounts aligned with seafloor spreading anomalies (Figure 4). However, the small wavelength and volumetric extent of these bodies impede their magnetic detection at the scale of the present survey.

In the area of the survey the Juan Fernández Ridge is represented not only by the O'Higgins group of seamounts but also by the Punta Salinas Ridge ending near the trench at Papudo seamount and by an extensive network of fractures paralleling these trends. Although the extrusives associated with the O'Higgins seamount are only 40 km wide, the flanking zone of parallel fractures is ~100 km wide. The wide distribution of large and small volcanic edifices on the seafloor (Figure 4) indicates a diffused magmatism distributed along multiple conduits. The discontinuity of the volcanic chain shows episodic volcanism.

The 3-D magnetic modeling shows that the episodic extrusive magmatism along the Juan Fernández trend is correlated with normal magnetic polarity. In fact, the timing assigned to the subducted Papudo seamount, the largest in the group, is coincident with one of the longest periods of normal polarity in the Cenozoic (anomaly 5). This observation could be explained by a sequence of magmatic pulses covering more than one period of reversals, with a small net remanence magnetization compared to the induced or viscous component. However, this is less likely than a dominant normal remanence, in which case this situation may not be just circumstantial. The large-scale relationship between the Cretaceous long normal polarity and the occurrence of superplumes [e.g. *Larson and Olson*, 1991] may be repeated here at a smaller scale. To establish such a smaller-scale relationship requires a high-resolution timing that is not yet available. The high magmatic productivity around the normal period of anomaly 5 is consistent with the dating of *O'Connor et*

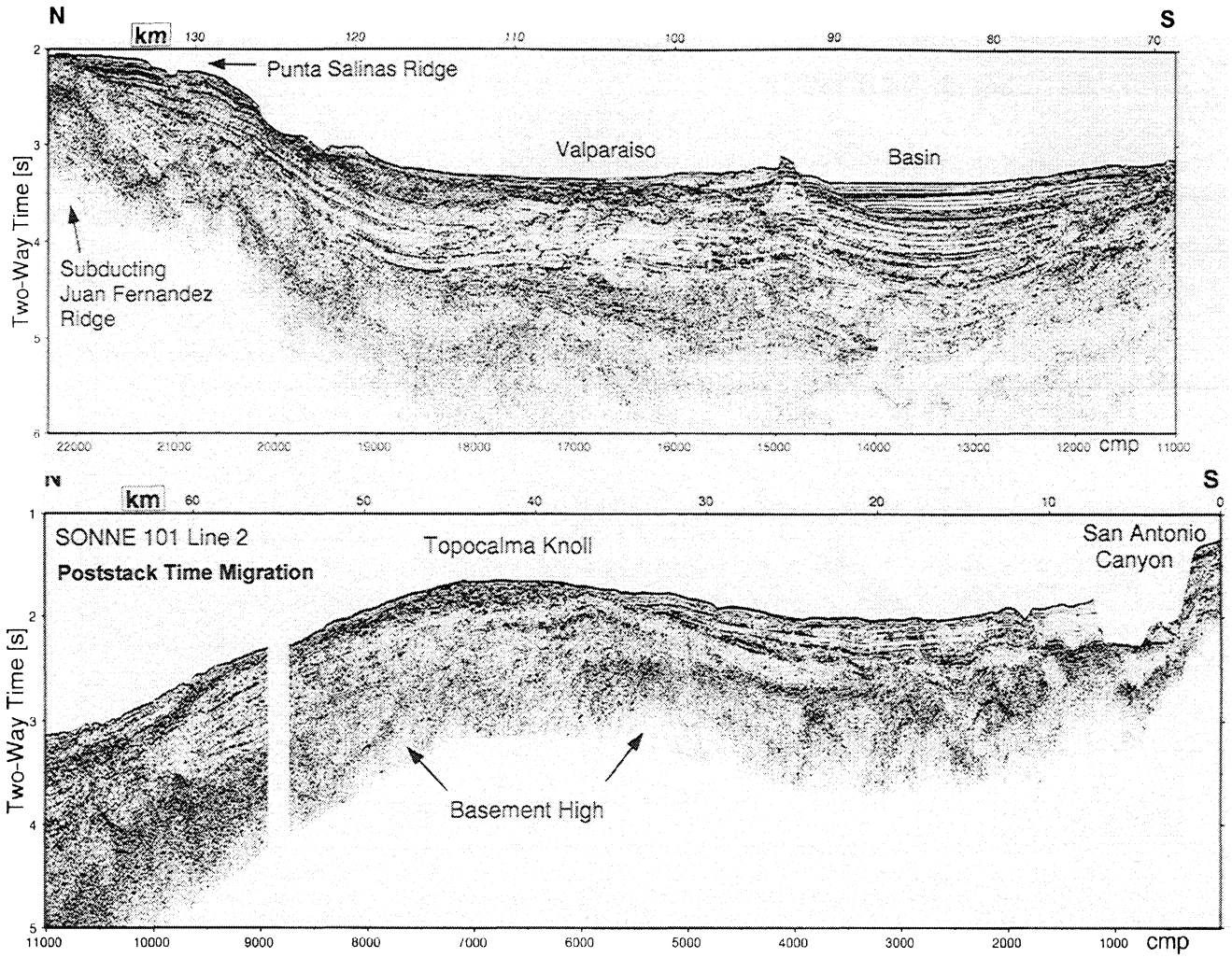

Figure 14. High-resolution multichannel seismic record SO101-2 running along the Topocalma Knoll and Valparaiso Basin. Note the uplift of oldest strata overlying acustic basement (continental crust) at the Topocalma Knoll and the unconformities bounding younger sedimentary units.

al. [1995] for the Easter chain farther north. In this case the extrusive products are also concentrated around a period of normal magnetic polarity.

4.1.2. Continental margin domain. This domain, between the trench and the coast is ~100 km wide (Figures 15 and 16). The continental margin is characterized by magnetic anomalies of 50 to 100 km wavelength and intermediate to low intensities (10 to 100 nT). These anomalies are associated with deeper or edge effect sources. On the continental side, east-west and west-northwest trends follow the main structural pattern of the continent. A correlation between magnetic pattern and morphology includes the Valparaiso Basin, bounded on the south by Topocalma Knoll (a positive magnetic anomaly), and by the northeast trending Punta Salinas Ridge, which is part of the Juan Fernández chain [*von Huene et al.*, 1997]. The positive anomalies associated with topographic highs around the San Antonio canyon reflect the presence of moderate strength magnetic sources and their well-developed north and south boundaries. However, the tectonic relationship between the lower reaches of San Antonio canyon and the associated magnetic anomalies is not yet understood. The seaward end of continental anomalies follows the general trend of the coast (Figure 16) and corresponds generally with the end of Mesozoic metamorphic rocks interpreted from seismic refraction and reflection data [*Flueh et al.*, 1998].

Magnetic anomalies that characterize the ocean crust show a dramatic decrease in amplitude east of the trench. Three-dimensional magnetic modeling (Figure 9) shows that the attenuation of seafloor anomalies is related to the increase in depth to the magnetic source of the subducting ocean lithosphere. The zone of attenuation follows the westward bend of the trench south of Valparaiso. As we can see in the refraction results shown in Figure 10, the subducting slab flexes into the trench at a steeper angle reflecting loading of the plate by trench sediment to the south, in contrast to the more buoyant slab associated with Juan Fernández Ridge to the north.

The single most prominent anomaly associated with the subducted oceanic crust is the Papudo seamount (Figure 15). This circular anomaly has a wavelength of ~30 km and an intermediate positive intensity of 50-100 nT. The causative body is at least equivalent to the O'Higgins seamount group. However, the scar left when it was subducted at the front of the margin has probably closed rapidly, leaving a ~10-km-wide mark (Figure 4). Such a behavior implies a very soft rheology in the accretionary prism.

The end of continental crust (see Figures 15 and 16) is indicated magnetically as a north-south series of small anomalies subparallel to the trench axis (Figure 16). To the north of 33°S, this boundary separates two main domains: (1) a western magnetic pattern of intermediate wavelengths and intensities and (2) a small magnetic intensities of long wavelength to the east.

The Valparaiso forearc basin has a minimum of 2-km-thick sediment in the northern section and probably more than 4 km in its southern side (Figure 13). On the other hand, sediment cover south of Valparaiso is only 1 to 2 km thick. Magnetic trends, like the Topocalma Knoll, represent the seaward continuation of Paleozoic intrusives and the associated structures (Figure 16).

High-resolution multichannel seismic reflection data across the Topocalma knoll and the Valparaiso Basin show that the knoll has been formed by uplift of a continental crust block (Figure 14). The lower strata are uplifted and folded with the continental basement, and it is overlaid unconformably by younger sediment units. The oldest strata can be followed to the north into the Valparaiso Basin.

Relatively indistinct rounded anomalies are aligned in a north south direction along the continental shelf and upper slope (Figure 16). Even though anomalies are of low amplitude, probably due to a longer time exposure to alteration and erosion, the alignment of anomalies resembles the magnetic lineations observed along exposed magmatic arcs onshore. We suggest that this north-south magnetic lineation could represent an abandoned arc of pre-Jurassic age, indicating a bound for the continental crust. This statement is based on the following lines of reasoning: (1) migration of the arc has been mostly eastward since at least Middle Jurassic times [Mpodozis and Ramos, 1989] and (2) unlike the subaerial arc-related magmatism, this suspected older magmatic relict appears to be cut by the tectonism associated with the rigid block of the Topocalma Knoll. If this interpretation is correct, it implies a fairly continuous process of magmatism and tectonic erosion of the margin since early Jurassic time.

Wide-angle seismic data across the margin show that the lineament of magnetic maximum is coincident with the seaward terminus of high-velocity bodies (Figure 10, velocities>6.5 km/s on upper plate) [*Flueh et al.*, 1998], supporting the hypothesis that the magnetic anomalies delineate the western edge of the continental plate.

The continental basement edge is located beneath the Valparaiso Basin and beneath the middle slope to the south (Figures, 10, 15, and 16). Seaward, a low-velocity body [*Flueh et al.*, 1998; *Zelt et al.*, 1999] forms a >40-km-wide prism of accreted sediment accumulated against the continental framework backstop. Sediment accretion is currently active to the south of the collision point as indicated by trench parallel elongated ridges at the base of the continental slope (Figure 4) formed by thrusting of the trench tubiditic infill. Deep penetrating seismic reflection data show that the low-velocity accretionary body is formed by thrusting and thickening of sediment packages [*Flueh et al.*, 1998], but the age of the sediment abutting the continental framework is unkown and thus the age of the beginning and the rate of accretion are unconstrained. A similar accretionary prism has been described southward along the margin [*Bangs and Cande*, 1997]. The forearc basins (e.g., Valparaiso Basin) have formed above the edge of the continental basement and are bounded seaward by the accretionary prism.

4.1.3. Subaerial crust domain. The continental crust domain includes the subaerial continental crust segment bounded to the east by the central depression (Figure 3). It is characterized by magnetic anomalies with a broad spectrum of intensities and wavelengths (Figure 7). Long-wavelength magnetic anomalies

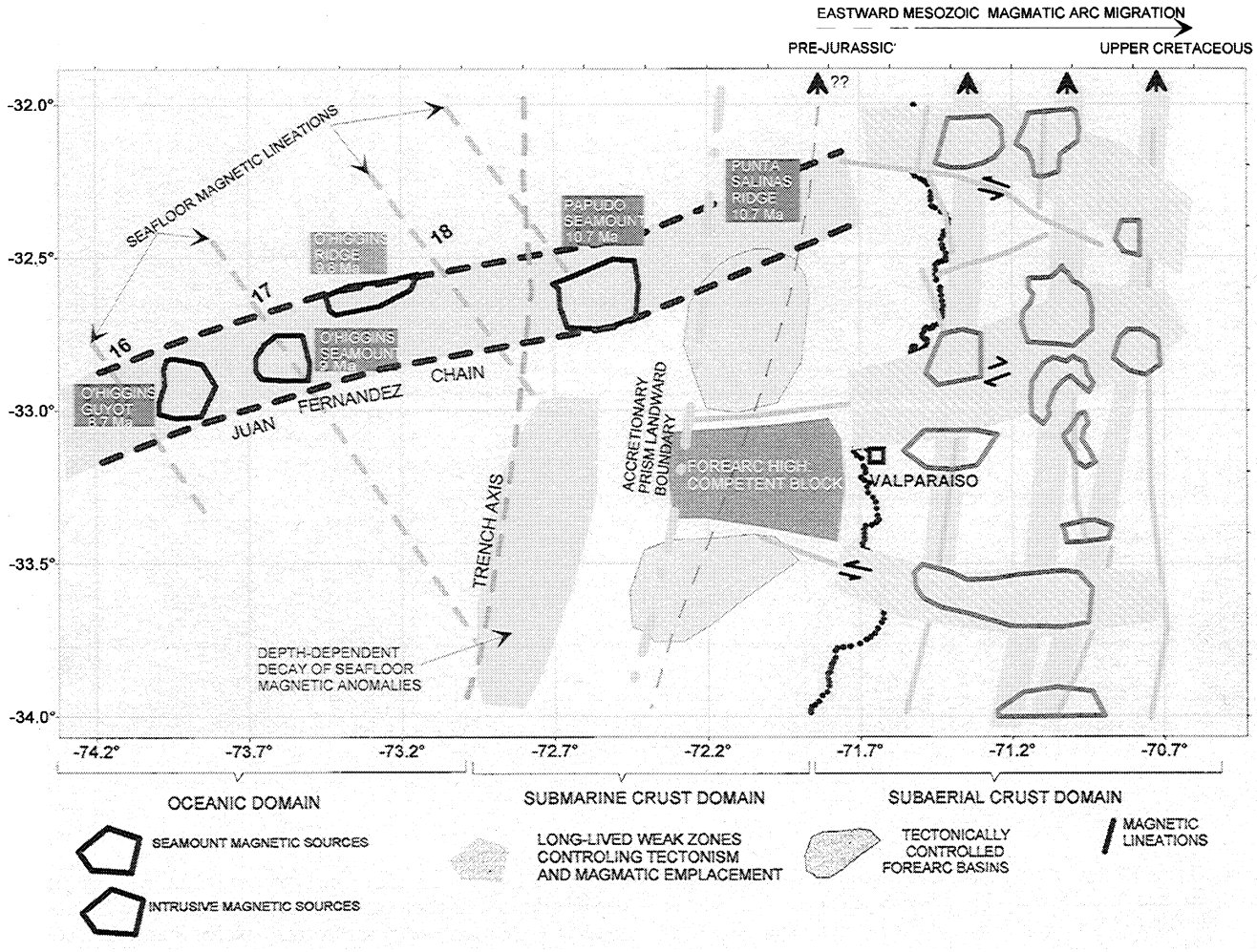

Figure 15. Tectonic interpretation and magnetic domain definition.

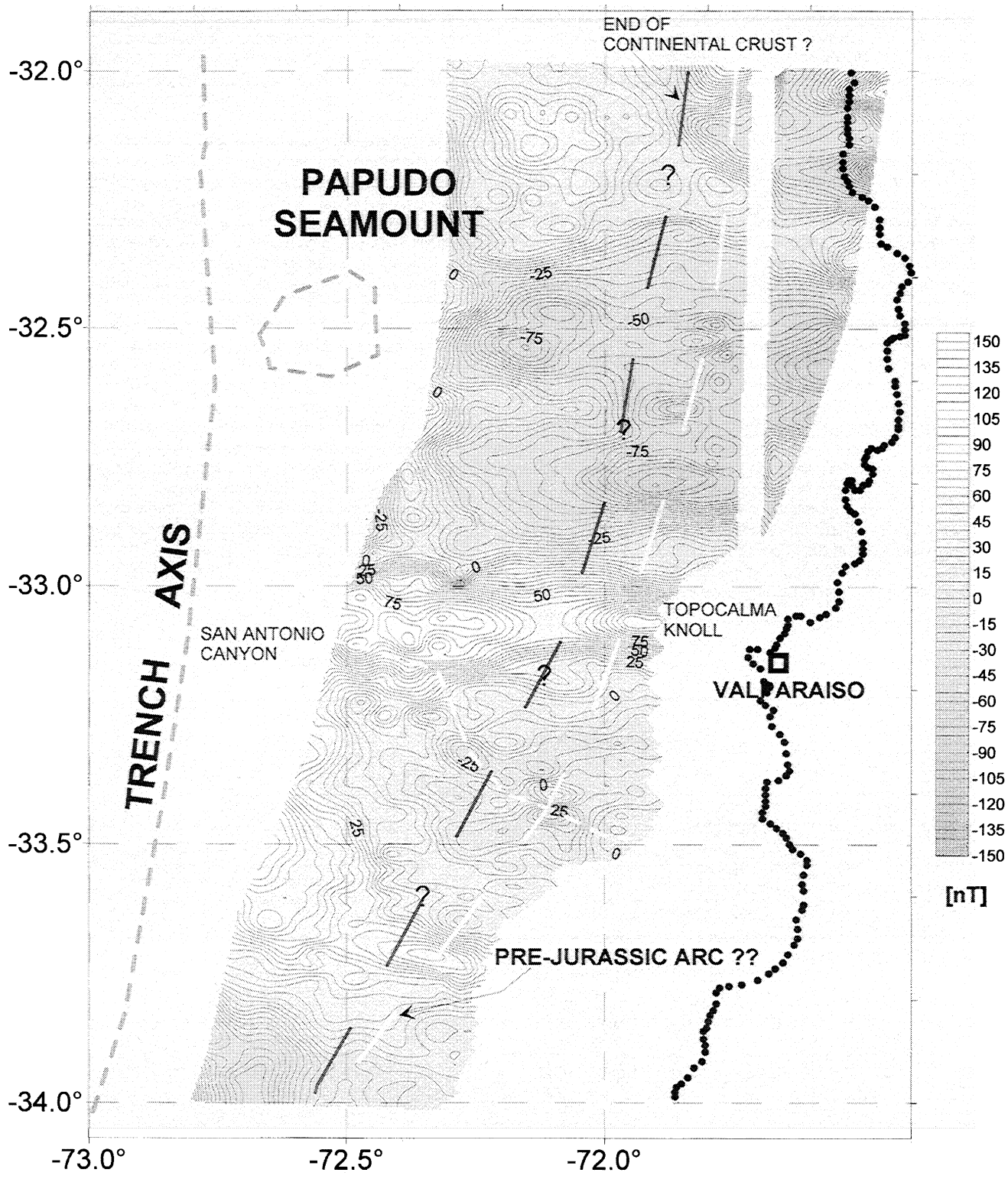

Figure 16. A larger view of the submarine continental domain showing an enhancement of a series of rounded anomalies aligned roughly N-S and interpreted as a suscpected pre-Jurassic arc (dashed with line). The end of the continental crust is also interpreted at the western edge of the suspected pre-Jurassic arc (dashed solid line).

(>30 km), associated with large and deep magnetic sources, overlap near field anomalies of high intensity and shorter wavelength (>5 km), as a direct result of a continuous process of magmatic intrusion at different crustal levels. Within this heterogeneous and overprinted magnetic field, three distinctive magnetic signatures characterize the domain:

1. Broad (> 30 km) and intense (>200 nT) magnetic anomalies (see location of the main bodies in Figure 15) cover almost all the continental section and involve Mesozoic igneous rocks with a clear eastward age migration [e.g., *Gana et al.*, 1994] (Figure 13). These anomalies belong to a conspicuous family of large magnetic anomalies, separated by an average

distance of 50-100 km along the margin [e.g., *Parra and Yáñez*, 1988]. According to *Yáñez and Maksaev* [1994] they probably represent broad areas in which most of the Mesozoic magmatism is concentrated.

2. A well-defined set of moderate-sized (5-15 km), near circular, magnetic anomalies along N-S trends (Figure 7), is found in the eastern flank of the Coastal Cordillera (Figure 3), mostly involving Upper Cretaceous intrusives [*Parra and Yáñez*, 1988) (Figures 13 and 15).

3. E-W to WNW and WSW set of subparallel magnetic lineations crossing the whole domain and extending towards the submarine crust domain (Figure 15) and beyond the study area eastward [*Yáñez et al.*, 1998]. The most conspicuous anomaly in this family, the Melipilla Anomaly (-33° 30' in Figure 7), has been interpreted in terms of a tabular and almost flat igneous body intruded along zones of weakness in the upper crust [*Gana et al.*, 1994; *Yáñez et al.*, 1998]. Consequently, other sectors of the domain in which this almost E-W magnetic pattern involves intrusive bodies of different ages can be interpreted as long-lived zones of weakness that favored magmatic emplacement and tectonism.

Unlike the observations in the previous domains (with the exception of the Juan Fernández Ridge), in the subaerial domain there is a strong correlation between magnetic anomalies and topography (compare Figures 3 and 7). A simple explanation for this strong link concerns the nature of the magnetic sources, mostly exposed intrusive rocks. These uplifted and eroded old rocks are in general isolated, in this way allowing a well-developed boundary in their north and south faces against nonmagnetic country rocks.

4.2. Comparative Analysis Between Magnetic Domains

The comparative analysis between different magnetic fabrics and geological units within this segment of the Andean convergent margin shows some distinctive features in the two end-members: subaerial and oceanic domains. However, they also share some common characteristics. In terms of magnetic intensities, or the corresponding magnetization of the causative bodies (see the pseudosusceptibility map of Figure 8), both domains show mean values consistent with medium to highly magnetized intrusive rocks of intermediate to mafic composition [e.g., *Telford et al.*, 1990]. Such a conclusion in the oceanic fabric is certainly expected; however, in the continental crust it points toward highly differentiated magma chambers [e.g. *Shieve et al.*, 1992]. In the continental margin domain the highly magnetized sources are probably enhanced by extensive erosional processes along the Coastal Cordillera since Mesozoic times, allowing the exposure of the intermediate to mafic nucleus at shallower crustal levels.

The correlation between topography/bathymetry and magnetic field is generally strong in the continental domain and low in the oceanic domain. Subaerial erosion seems to be an important controlling factor allowing the exposure of hard and highly magnetized intrusive rocks in the former. In contrast, we observe a fairly homogeneous distribution of the extrusive layer in the oceanic domain. The most remarkable positive correlation of bathymetry and magnetic anomalies is observed at the Juan Fernández chain. These prominent volcanic edifices generate strong and isolated magnetic anomalies in very much the same style as the exposed intrusives along the Coastal Cordillera on land.

4.3. Tectonic Implications of the Juan Fernández Ridge Interaction with the Andean Margin

One focus of the study in the Valparaiso area is the effect of the subducting Juan Fernández Ridge on the upper plate. Ridges intersecting continental margins are areas of major uplift and local tectonic erosion in the collision zone. Until the Chilean margin opposite the Juan Fernández Ridge was comprehensively explored, it was assumed that the ridge continued beneath the continent along its essentially eastward trend. This trend coincides with the end of active volcanism as observed where ridges subduct elsewhere. However, satellite gravity maps and swath mapping [*Sandwell and Smith*, 1995] made it clear that the ridge departs from its east-west trend near the O'Higgins seamount and swings northeast. The bathymetric trend of the seamounts and many fractures reactivated as the ridge enters the trench all have a N60°E trend, nearly at right angles to the trend of magnetic anomalies [*von Huene et al.*, 1997]. This deviation of the ridge trend is greater than the deviation along the farther north coeval Sala y Gomez Ridge at 8 Ma, located farther north. This more northerly alignment of the trends associated with the Juan Fernández Ridge was problematic in the study of *von Huene et al.* [1997]. The change in plate direction at ~25 Ma between the Sala y Gomez and Nazca ridges produced a wide and complex zone of hot spot-derived seafloor relief. It was speculated that a similarly complex juncture could have developed along the Juan Fernández Ridge during the 8 Ma plate motion change. However, according to *von Huene et al.* [1997] the most likely indication of the subducted ridge position was inconsistent with temporal and physical indicators.

Here we give less weight to morphological trends and develop an inferred trace of the subducted ridge that is more consistent with the tectonic configuration of the margin (Figure 1).The age determination for the O'Higgins volcanoes implies a specific plate reconstruction for the late Miocene (modified from *Gordon and Jurdy* [1986]). The absolute poles of rotation and angular velocities of the Nazca/Farallon and South America plates used in the plate reconstruction are given in Table 1. In Figure 17 we present the evolution of the Juan Fernadez hot spot chain since Miocene times, assuming a continuous magmatic activity. This plate reconstruction is basically consistent with the previous results of *Pilger* [1981, 1983], although the precise dating of the Juan Fernández Ridge now allows a better constrained timing for the ridge-continent interaction.

From the plate motion prediction the intersection where the Juan Fernández Ridge subducted beneath the continent has moved only 2.5° southward (~275 km) in the last 12 Myr. In contrast, during early Miocene time a southward migration of the intersection was an order of magnitude faster (~200 km/Myr). The margin was probably eroded, in particular to the north of 33°S, where tectonic erosion has been predominant during the Cenozoic. The subduction of a north-northeast aseismic ridge between 24 and 12 Ma coincides roughly in time with the geological evidence of volcanic quiescence at 20 Ma and an attenuated athenospheric wedge between ~26 and 28° S [*Kay et al.*, 1991]. Under this geometry the entire subducting slab lithosphere probably underwent a thermal resetting, favoring a more buoyant behavior. If magmatic production along the large igneous provinces is somehow a worldwide phenomenon [e.g., *Larson and Olson*, 1991], then the observed Nazca Ridge suggests a larger production along the coeval Juan Fernández Ridge (see location in Figure 2). This already subducted branch

Table 1. Poles of Rotation and Angular velocities for Nazca/Farallon and South American Plates[a]

Time, Ma	Nazca/Farallon Plate			South America Plate		
	Latitude	Longitude	Degree per million years	Latitude	Longitude	Degree per million years
64	-26	-62.7	-1.08	41.8	52.4	-0.308
56	-50.4	-27	-1.266	58.8	47.7	-0.297
48	-40.6	-51.8	-1.026	78.9	43.8	-0.392
43	-43.8	-26.6	-0.694	77.6	26.8	-0.187
25	-57.5	80.1	-0.742	80.5	-12.9	-0.119
10	-47.4	84.2	-0.856	79.1	-15.7	-0.113

[a]modified from Gordon and Jurdy [1986]

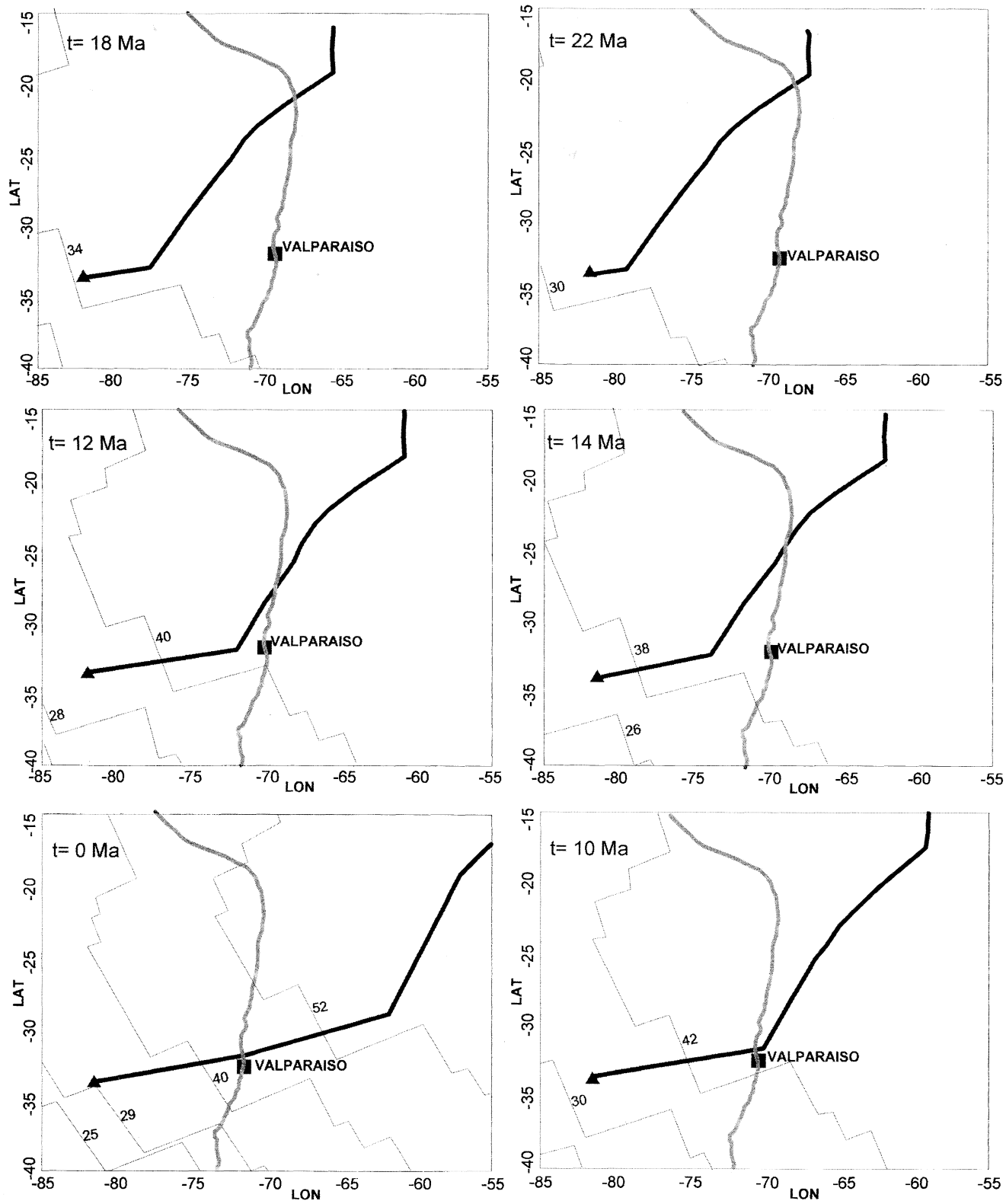

Figure 17. Predicted path for the Juan Fernández hot spot chain since Miocene times. The location of the hotspot is indicated by a solid triangle. The margin of South America (light solid line) moves westward, while the hot spot location remains stationary. Location of Valparaiso (solid square) is shown as a reference. Absolute plate motions from poles of rotations described in Table 1. Seafloor spreading magnetic lineations are indicated with their magnetic number.

of the Juan Fernández Ridge could further increase the buoyancy of the slab, allowing a more efficient process of slab shallowing. The southeastward migration of the subducted ridge would extend the flat slab segment until 12-10 Ma. The inferred subducted Juan Fernández chain (Figure 18) correlates with seismic hypocenters [*Kirby et al.*, 1996], and the depth to the Wadatti-Benioff plane [from *Cahill and Isacks*, 1991; *Kirby et al.*, 1996]. The tapered northern flank (~27°-28°S) of the flat slab area contrasts with the sharper flexure in its southern end (~33.5°S). The southward and eastward migration of the ridge can explain this asymmetry by subduction of a buoyant body.

The consequences of the model presented here are only partly tested with current data. During the last 10 Myr, the Juan Fernández Ridge intersection with the margin (Figure 4) was

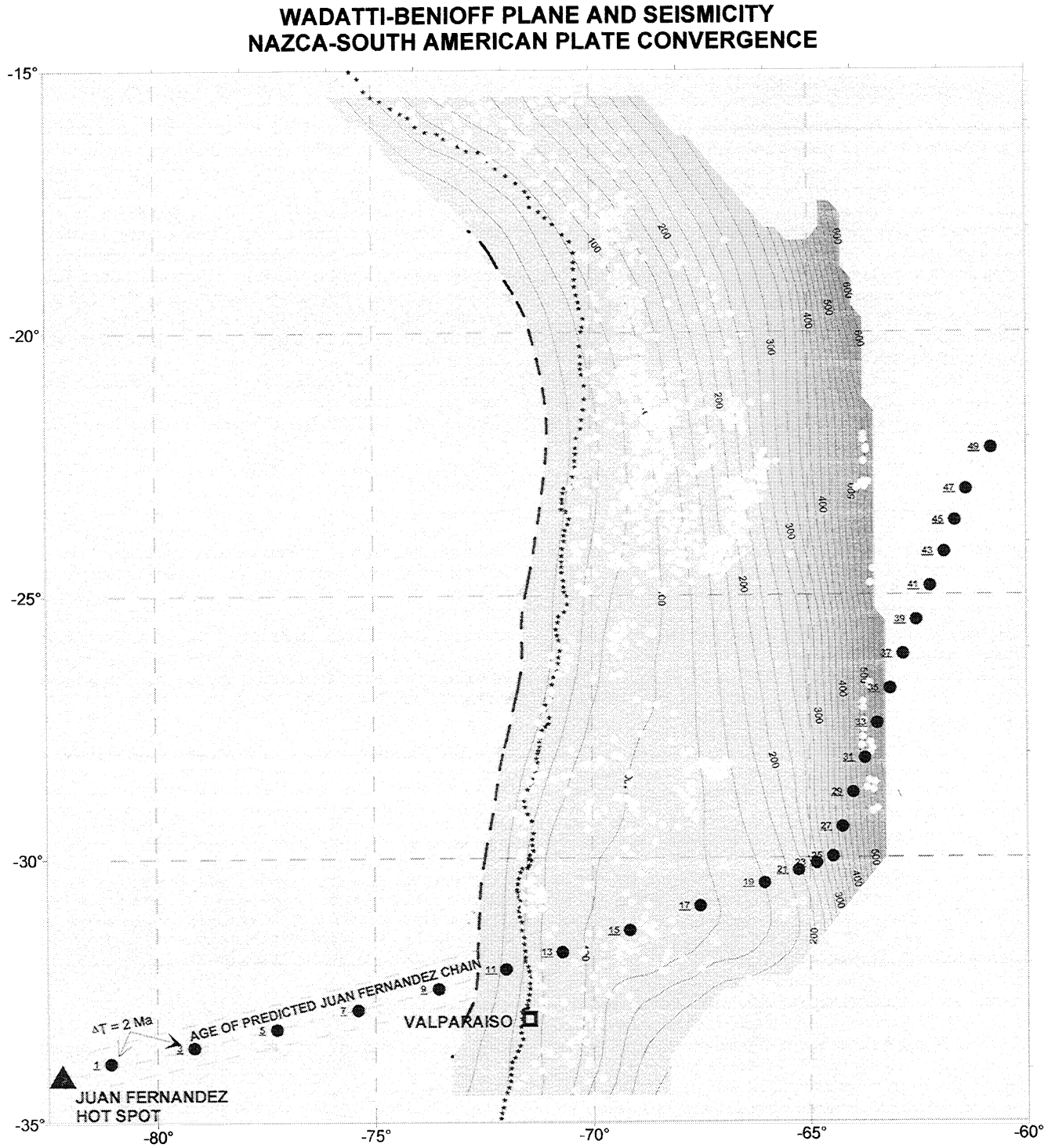

Figure 18. Predicted path of the Juan Fernández hot spot chain at present. Numbers along the path represent the age of the predicted volcanic events (Ma). Open dots are the observed seismicity [from *Kirby et al.*, 1996]. The contour lines show the depth to the Wadatti-Benioff plane [from *Cahill and Isacks*, 1992; *Kirby et al.*, 1996].

probably an efficient agent of sediment trap for the incoming sediments from the south. The abundance of trench sediment probably promoted construction of an accretionary prism along the margin to ~33°S latitude. In fact, the northern flank of the Valparaiso Basin is controlled by the subduction of the Juan Fernández Ridge, whereas its southern boundary corresponds to the topographic high of Topocalma knoll (Figure 3). This positive feature represents an extension of an old continental structure, probably activated in the past by right lateral strike-slip [*Yáñez et al.*, 1998]. This rigid block also coincides with the hypocenter of the 1985 earthquake [*Comte et al.*, 1986].

The spatial connection between the Juan Fernández Ridge and a major tectonic boundary in the continental plate suggests an even broader speculation. The long-lived segmentation of the continent at 33.5°S would be controlled by a quasi-stationary interaction with the magmatic products of the Juan Fernández hot spot. To the north of this tectonic boundary, tectonic erosion has dominated over accretion, and is currently active since perhaps Jurassic times [*Rutland*, 1971; *von Huene et al.*, 1999]. To the south, the smaller migration of the volcanic arc indicates a delicate balance between accretion and erosion over time. On the other hand, paleoreconstructions of the South American plate during the Meso-Cenozoic [e.g., *Scotese and Sager*, 1988] show little N-S displacement. Therefore most of its absolute plate motion has been in the E-W direction. The evolution of the Nazca-Farallon plate prior to Late Tertiary is not constrained. The only fragmentary evidence for a plate reconstruction is preserved in the conjugate area of the Pacific plate, indicating a tectonic fabric nearly at right angle with respect to the Nazca plate. However, the geological record at the continent shows evidence of an almost continuous record of normal subduction since at least Middle Jurassic [e.g.. *Mpodozis and Ramos*, 1989]. The associated subparallel seafloor spreading center in the proto-Pacific was probably more stable and prevailed during long periods of time. If we further assume a long-term magmatic production in the Juan Fernández hot spot, we can envision the built up of this major tectonic boundary as a result of the almost continuous interaction with a paleo-Juan Fernández Ridge in very much the same way as we observe it today. Although acknowledging that key elements to prove this hypothesis are definitely not present, geological evidence are at least consistent with this speculative interpretation.

5. Conclusions

Full coverage of regional magnetic information has been integrated along the western margin of South America between latitudes 32° and 34°S in a 400-km E-W transect. This transect covers parts of the oceanic and continental plates at a segment boundary of the Andes. For a better analysis and correlation of the magnetic fabric the data have been downward continued to 1000 m above the topography/bathymetry. This processing was accomplished using 2-D equivalent magnetic source representation and SVD analysis for high-frequency noise suppression. The 2-D model of the oceanic crust and the full 3-D model of the oceanic plate allowed a precise timing of the plate velocities during the Cenozoic sequence under analysis and also provided a good location, size definition, and timing for the hot spot-related Juan Fernández Ridge. Normal oceanic plate in this area was formed during the late Eocene-early Oligocene times (35-39 Ma) at a half spreading rate of 6 $mmyr^{-1}$. The Juan Fernández Ridge, including the Papudo subducted seamount, perturbed this magnetic sequence during the Miocene (8-11 Ma).

The joint analysis of the magnetic database and derived 2-D and 3-D models, topography/bathymetry, and reflection and refraction seismic profiles allowed the definition of three magnetic domains. Distinctive trends and features consistent with the main morphotectonic units of the area characterize each domain. The magnetic fabric of the oceanic domain is characterized by regular magnetic sources of NW orientation and consistently high magnetization. This domain is perturbed by the Juan Fernández Ridge hot spot, mostly emplaced during periods of normal polarity. In contrast, a heterogeneous magnetic fabric consistent with the geological diversity of the continental region characterizes the subaerial crust domain. A series of N-S and crossed E-W trends characterize the domain and extend beyond the shore. The continental margin domain, between these two end-members, is characterized by deep magnetic sources of low to moderate intensities, in agreement with the development of an accretionary prism and forearc basins. The magnetic contribution of the oceanic plate is restricted to the Papudo subducted seamount, and the eastward dipping subducting slab has a negligible effect. On the other hand, the contribution from the continental crust involves the series of E-W structures that underlay the east flank of Valparaiso Basin, probably exerting a tectonic control over its southern flank. A series of rounded anomalies aligned N-S at the axis of the forearc basins are interpreted as the presumably pre-Jurassic abandoned magmatic arc. The correlation between the topography and magnetic field is very high onshore, in the subaerial crust domain, where erosion exposed deep and highly magnetized intrusive bodies. Minor bathymetric lineaments reveal the fabric of the crust formed at the spreading ridge. The only strong correlation between major bathymetric relief and the magnetic field is observed along the Juan Fernández chain.

The relatively slow migration of the Juan Fernández Ridge along the continental margin during the past 10 Myr probably provided a barrier for the accumulation of trench sediments. Slow migration is probably important for the deep sediment section deposited in the Valparaiso Basin. The location of the basin southern flank is aligned with preexisting geological structures on the continent.

The paleoreconstruction of the Juan Fernández Ridge against the continental plate is consistent with the geological timing for the shallowing of the subducting slab. Present seismicity also correlates with the predicted location of the subducted ridge, further suggesting a relationship between the flat slab and the subducted ridge. Paleoreconstruction of the South American and the oceanic plates, although speculative, may suggest a long-lived influence of the Juan Fernández hot spot on the tectonics of the continental margin near 33.5°S.

Acknowledgments. Subroutines from the GMT package [*Wessel and Smith*, 1991] have been extensively used for the process of gridding. Geophysical package used in the 2-D and 3-D magnetic modeling and processing have been kindly provided by GEODATOS. The marine magnetic data were acquired by the R/V *Sonne*, during the Condor project cruise funded by the German BMBF under project 03G0103A. The final part of the processing and writing of this paper have been possible by a DAAD scholarsip granted to one of the authors (G.Y.). We thank D. Klaeschen and Jane Laursen for processing seismic data SO101 line 2 shown on Figure 14. We thank Steve Cande, John LaBrecque, and Augusto Rapalini for a careful review of the article. This paper has been partially supported by FONDECYT grant 1000136.

References

Bangs, N.L., and S. Cande, The episodic development of a convergent margin inferred from structures and processes along the southern Chile margin, *Tectonics*, *16*, 489-505, 1997.

Barazagni, M., and B.L. Isacks, Spatial distribution of earthquakes and subduction of the Nazca plate beneath South America, *Geology*, *4*, 686-692, 1976.

Cahill, T., and B.L. Isacks, Seismicity and shape of the subducted Nazca plate, *J. Geophys. Res.*, *97*, 17,503-17,529, 1992.

Cande, S.C., and W.F. Haxby, Eocene propagating rifts in the southwest Pacific and their conjugate features on the Nazca plate, *J. Geophys. Res.*, *96*, 19,609-19,622, 1991.

Cande, S.C., and D.V. Kent, Revised calibration of the geomagnetic timescale for the Late Cretaceous and Cenozoic, *J. Geophys. Res.*, *100*, 6093-6095, 1995.

Cande, S.C., and R.B. Leslie, Late Cenozoic tectonics of the southern Chile trench, *J. Geophys. Res.*, *91*, 471-496, 1986.

Cande, S.C., J.L. Labrecque, R.L. Larson, W.C. Pitman III, X. Golovchenko, and W.F. Haxby, *Magnetic Lineations of the World's Ocean Basins*, Am. Assoc. of Pet. Geol., Tulsa, Okla., 1989.

Comte, D., A. Eisemberg, E. Lorca, M. Pardo, L. Ponce, R. Saragoni, S.K. Sing, and J.G. Suarez, The great 1985 central Chile earthquake: A repeated of previous great earthquake in the region?, *Science*, *233*, 449-453, 1986.

Davidson, J., and C. Mpodozis, Regional geological setting of epithermal gold deposits, Chile, *Econ. Geol.*, *86*, 1174-1186, 1991.

DeMets, C., R.G. Gordon, D.F. Argus, and S. Stein, Current plate motions, *Geophys. J. Int.*, *101*, 425-478, 1990.

Flueh, E.R., et al., Seismic investigation of the continental margin off- and onshore Valparaiso, Chile, *Tectonophysics*, *288*, 251-263, 1998.

Gana, P., G.A. Yáñez, R. Wall, Evolución geotectónica de la Cordillera de la Costa del Chile central (33-34°S): Control Geológico y Geofisico, *Actas Congr. Geol. Chileno*, *VII*, 38-42, 1994.

Gana, P., R Wall, and A. Gutierrez, Mapa geológico del area Valparaiso-Curacavi, regiones de Valparaíso y Metropolitana, *Mapas Geol. 1*, scale 1:100,000, Serv. Nac. de Geol. y Min., Santiago, Chile, 1996.

Gordon, R.G., and D.M. Jurdy, Cenozoic global plate motions, *J. Geophys. Res.*, *91*, 12,389-12,406, 1986.

Hansen, R.O., and Y. Miyazaki, Continuation of potential fields between arbitrary surfaces, *Geophysics*, *49*, 787-795, 1984.

Harrison, C.G. A., Marine magnetic anomalies–the origin of the stripes, *Annu. Rev. Earth Planet. Sci. 15*, 505-543, 1987.

Jordan, T.E., B. Isacks, R. Allmendinger, J. Brewer, V.A. Ramos, and C. Ando, Andean tectonics related to the geometry of subducted plates: *Geol. Soc. Am. Bull.*, *94*, 341-361, 1983.

Kay, S.M., C. Mpodozis, V.A. Ramos, and F. Munizaga, Magma source variations for mid-late Tertiary magmatic rocks associated with a shallowing subduction zone and the thickening crust in the central Andes (28-33° S), *Spec. Pap. Geol. Soc. Am.*, *265*, 113-137, 1991.

Kirby, S., E.R. Engdahl, and R. Denlinger, Intermediate-depth intraslab eartquakes and arc volcanism as physical expressions of crustal and uppermost mantle metamorphism in subducting slab, in *Subduction Top to Bottom*, *Geophys. Monogr. Ser.*, vol. 96, edited by G. Bebout et al., pp.195-214, AGU, Washington, DC, 1996.

Larson, R.L., and P. Olson, Mantel plumes control magnetic reversal frequency, *Earth Planet. Sci. Lett.*, *107*, 437-447, 1991.

Molnar, P., and P. England, Temperatures, heat flux, and frictional stress near major thrust faults, *J. Geophys. Res.*, *95*, 4833-4856, 1990.

Mpodozis, C., and V. Ramos, The Andes of Chile and Argentina, in *Geology of the Andes and Its Relations to Hydrocarbon and Mineral Resources*, *Earth Sci. Ser., vol 11*, edited by G.E. Ericksen, M.T. Cañas Pinochet, and J.A. Reinemund, pp. 59-90, Circum-Pac. Counc. for Energy and Miner. Resour., Houston, Texas, 1989.

Noble, B., and J.W. Daniel, *Applied Linear Algebra*, 477 pp., Prentice-Hall, Englewood Cliffs, N.J., 1977.

Nur, A., and Z. Ben-Avraham, Volcanic gaps and the consumption of aseismic ridges in South America, *Mem. Geol. Soc. Am.*, *154*, 729-740, 1981.

O'Connor, J.M., P. Stoffers, and M. O. McWilliams, Time-space mapping of Easter Chain volcanism, *Earth Planet. Sci. Lett.*, *136*, 197-212, 1995.

Pardo-Casas, F., and P. Molnar, Relative motion of the Nazca (Farallon) and South American plates since Late Cretaceous time, *Tectonics*, *6*, 233-248, 1987.

Parra, J.C., and G.A. Yáñez, Provincias magnéticas del Chile central. *Rev. Geol. Chile*, *15*, 101-117, 1988.

Pilger, R.H., Plate reconstructions, aseismic ridges, and low angle subduction beneath the Andes, *Geol. Soc. Am. Bull.*, *92*, 448-456, 1981.

Pilger, R.H., Kinematics of the South American subduction zone from global plate reconstructions, in *Geodynamics of the Eastern Pacific Region, Caribbean and Scotia Arcs*, *Geodyn. Ser.*, vol. 9, edited by R. Cabré, pp. 113-125, AGU, Washington, D.C., 1983.

Plouff, D., Gravity and magnetic fields of polygonal prisms and application to magnetic terrain corrections, *Geophysics*, *41*, 727-741, 1975.

Rivano, S., P. Sepúlveda, M. Hervé, and A. Puig, Geocronología K-Ar de las rocas intrusivas entre los 31°-32° latitud sur, Chile, *Rev. Geol. Chile*, *24*, 63-74, 1985.

Rivano, S., E. Godoy, M. Vergara, and R. Villarroel, Redefinición de la Formación Farellones en la Cordillera de los Andes de Chile central (32-34°S), *Rev. Geol. Chile*, *17*, 205-214, 1990.

Rutland, R.W.R., Andean orogeny and ocean floor spreading, *Nature*, *233*, 252-255, 1971.

Sandwell, D., and W.H.F. Smith, Gravity anomaly Geosat and ERS-1 altimetry, version 6.0, Geol. Data Cent., Scripps Inst. of Oceanogr. La Jolla, Calif., 1995.

Scotese, C.R., and W.W. Sager, Mesozoic and Cenozoic plate tectonic reconstructions. *Tectonophysics*, *155*, 27-48, 1988.

Shieve, P.N., R.J. Blakely, B.R. Frost, and D.M. Fountain, Magnetic properties of the lower continental crust, in *Continental Lower Crust*, edited by D.M. Fountain, R. Arcukus, and R.W. Kay, pp. 145-170, Elsevier Sci., New York, 1992.

Sillitoe, R.H., Tectonic segmentation of the Andes: Implications for magmatism and metallogeny, *Nature*, *250*, 542-545, 1974.

Stern, C.R., and C. Mpodozis, Geologic evidence for subduction erosion along the west coast of central and northern Chile, *Actas Congr. Geol. Chileno*, *VI* (1), 205-207, 1991.

Telford, W.M., L.P. Geldart, and R.E. Sheriff, *Applied Geophysics* 2nd ed., 770 pp., Cambridge Univ. Press, New York, 1990.

von Huene, R., and D.W. Scholl, Observations at convergent margins concerning subduction, subduction erosion and the growth of continental crust, *Rev. Geophys.*, *29*, 279-316, 1991.

von Huene, R., J. Corvalán, and K. Korstgard, *Cruise Report SO101 Condor*, 171 pp., GEOMAR, Kiel, Germany, 1995.

von Huene, R., J. Corvalán, E.R. Flueh, K. Hinz, J. Korstgard, C.R. Ranero, W. Weinrebe, and the Condor Scientists, Tectonic control of the Juan Fernández Ridge on the Andean margin near Valparaiso, Chile, *Tectonics*, *16*, 474-488, 1997.

von Huene, R., W. Weinrebe, and F. Heeren, Subduction erosion along the North Chile margin, *J. Geodyn.*, *27*, 345-358, 1999.

Wessel, P., and W.H. Smith, Free software helps map and display data, *Eos Trans. AGU*, *72*, 441, 445-446, 1991.

Yáñez, G.A., A thermo-viscous model for the long-lived segmentation of the southern Andes geological evolution, Ph.D. Thesis, Columbia Univ., New York, 1995.

Yáñez, G., and J. LaBrecque, Age dependent three dimensional magnetic modeling of the North Pacific and North Atlantic oceanic crust at intermediate wavelengths, *J. Geophys. Res.*, *102*, 7947-7961, 1997.

Yáñez, G.A. and V. Maksaev, Sobre la distribución espacial de cuerpos intrusivos asociados a diapirismo y la caracterización de la fuente magmática en pórfidos cupríferos: Inestabilidades gravitacionales en un medio viscoso, *Actas Congr. Geol. Chileno*, *VII*, 1642-1646, 1994.

Yáñez, G.A., C.R. Ranero, and J. Díaz, Magnetic survey: Instrumentation, data acquisition, processing, modeling and interpretation, *Cruise Report SO101 Condor*, pp. 31-61, GEOMAR, Kiel, Germany, 1995.

Yánez, G., P. Gana, and R. Fernández, Origen y significado geologico de la Anomalia Melipilla, Chile central, *Rev. Geol. Chile*, *25*, 175-198, 1998.

Zelt, C., A. Hojka, E.R. Flueh, and K. Mcintosh, 3D simultaneous seismic refraction and reflection tomography of wide angle data from the central Chilean margin, *Geophys. Res. Lett.*, *26*, 2577-2580, 1999.

J. Díaz, Universidad Católica de Valparaíso, Av. Altamirano 1480, Valparaíso, Chile. (jdiaz@ucv.cl)

C. R. Ranero, and R. von Huene, GEOMAR, Christian Albrechts Universität, 24148 Kiel, Germany. (cranero@geomar.cl)

G. A. Yáñez, GEODATOS SAIC, Román Díaz 773, Santiago, Chile. (goyanez@geodatos.cl)

(Received September 22, 1999; revised August 29, 2000;
accepted September 7, 2000)